JEM Journal of Experimental Medicine

BRIEF DEFINITIVE REPORT

Elongated neutrophil-derived structures are blood-borne microparticles formed by rolling neutrophils during sepsis

Alex Marki[1], Konrad Buscher[1,2], Cristina Lorenzini[1,3], Matthew Meyer[1], Ryosuke Saigusa[1], Zhichao Fan[1,4], Yi-Ting Yeh[5], Nadine Hartmann[1], Jennifer M. Dan[1,6], William B. Kiosses[1], Gregory J. Golden[7], Rajee Ganesan[8], Holger Winkels[1], Marco Orecchioni[1], Sara McArdle[1], Zbigniew Mikulski[1], Yoav Altman[9], Jack Bui[10], Mitchell Kronenberg[1], Shu Chien[13], Jeffrey D. Esko[7], Victor Nizet[11], David Smalley[12], Johannes Roth[13], and Klaus Ley[1,14]

Rolling neutrophils form tethers with submicron diameters. Here, we report that these tethers detach, forming elongated neutrophil-derived structures (ENDS) in the vessel lumen. We studied ENDS formation in mice and humans in vitro and in vivo. ENDS do not contain mitochondria, endoplasmic reticulum, or DNA, but are enriched for S100A8, S100A9, and 57 other proteins. Within hours of formation, ENDS round up, and some of them begin to present phosphatidylserine on their surface (detected by annexin-5 binding) and release S100A8–S100A9 complex, a damage-associated molecular pattern protein that is a known biomarker of neutrophilic inflammation. ENDS appear in blood plasma of mice upon induction of septic shock. Compared with healthy donors, ENDS are 10–100-fold elevated in blood plasma of septic patients. Unlike neutrophil-derived extracellular vesicles, most ENDS are negative for the tetraspanins CD9, CD63, and CD81. We conclude that ENDS are a new class of bloodborne submicron particles with a formation mechanism linked to neutrophil rolling on the vessel wall.

Introduction

Neutrophils protect the host from invading bacteria by arriving at the site of infection and engaging in antibacterial secretory and phagocytic activities (Christoffersson and Phillipson, 2018; Gómez-Moreno et al., 2018; Soehnlein et al., 2017). Neutrophils mature in the bone marrow and travel in the blood circulation, surveilling for infectious or inflammatory signals (Ley et al., 2018; Nourshargh and Alon, 2014). Upon sensing such signals, the neutrophils roll and arrest on the endothelium and eventually migrate across the vessel wall into the inflamed tissue. Neutrophil rolling is enabled by intermittent bond formation between endothelial selectins and their ligands on the neutrophil (Ley et al., 2018; Nourshargh and Alon, 2014), with a contribution from β2 integrins on the neutrophils and their ligands on the endothelial cells (Ley et al., 2018). Rolling is stabilized by formation of tethers, which are long, ∼200-nm-thin structures extending from the adhered microvilli of rolling neutrophils (Marki et al., 2016, 2018; Sundd et al., 2012).

During this recruitment process, neutrophils undergo gradual activation and may already begin to discharge antibacterial compounds in membrane packages or freely, as suggested by the presence of primed neutrophils (Fine et al., 2019), neutrophil-derived extracellular vesicles (EVs; Timár et al., 2013), and neutrophil extracellular traps (NETs; Colón et al., 2019) in blood. Release of different EVs (Colombo et al., 2014; Maas et al., 2017; van Niel et al., 2018) includes 30–100-nm large exosomes, formed by multivesicular body fusion with the plasma membrane. The 200–500-nm large ectosomes (or microvesicles) bud off directly from the plasma membrane into the extracellular

[1]La Jolla Institute for Immunology, La Jolla, CA; [2]Division of General Internal Medicine, Nephrology, and Rheumatology, Department of Medicine D, University Hospital Muenster, Muenster, Germany; [3]Laboratory of Immunobiology, Federal University of Santa Catarina, Florianopolis, Santa Catarina, Brazil; [4]Department of Immunology, University of Connecticut Health Center, Farmington, CT; [5]Mechanical and Aerospace Engineering, University of California, San Diego, La Jolla, CA; [6]Division of Infectious Diseases and Global Public Health, University of California, San Diego, La Jolla, CA; [7]Department of Cellular and Molecular Medicine and Glycobiology Research and Training Center, University of California, San Diego, La Jolla, CA; [8]Department of Biology, University of North Carolina at Chapel Hill, Chapel Hill, NC; [9]Sanford Burnham Prebys Medical Discovery Institute, La Jolla, CA; [10]Department of Pathology, University of California, San Diego, La Jolla, CA; [11]Department of Pediatrics and Skaggs School of Pharmacy and Pharmaceutical Sciences, University of California, San Diego, La Jolla, CA; [12]Systems Mass Spectrometry Core, Parker H. Petit Institute for Bioengineering and Bioscience, Georgia Institute of Technology, Atlanta, GA; [13]Institute for Immunology, University of Muenster, Muenster, Germany; [14]Department of Bioengineering and Institute of Engineering in Medicine, University of California, San Diego, La Jolla, CA.

Correspondence to Klaus Ley: klaus@lji.org.

space, whereas large apoptotic bodies (up to several micrometers in diameter) bud off from apoptotic cells. Neutrophil-derived EVs are recognized by their submicron size and their neutrophil-specific surface marker, CD66b. The general EV surface markers phosphatidylserine (PS; Timár et al., 2013) and CD63 tetraspanin (TS; Genschmer et al., 2019) were also detected on neutrophil-derived EVs (Hong, 2018). Using imaging cytometry, Headland et al. (2014) found that healthy human blood plasma contains ∼2,500 EVs/µl, of which 12% are leukocyte derived ($CD45^+$) and 3.6% are neutrophil derived ($CD66b^+$). In culture, both suspended and adhered human neutrophils release EVs (Dalli et al., 2013; Headland et al., 2014; Timár et al., 2013; Lőrincz et al., 2015). Stimulation with inflammatory mediators increases the EV release rate and alters the EV composition (Headland et al., 2014; Timár et al., 2013; Johnson et al., 2014). Extravasated neutrophils also release compounds in migrasomes. These plasma membrane–covered microparticles detach from the neutrophil's uropod as the neutrophil migrates across the vessel wall or in the tissue (Hyun et al., 2012; Lim et al., 2015). The main membrane-free release mechanism of neutrophils is degranulation, a special form of exocytosis, where the contents of neutrophil granules (intracellular vesicles) are released via granule fusion with the plasma membrane (Ley et al., 2018). Another membrane-free inflammatory mediator discharge mechanism is the release of NETs, nuclear or mitochondrial DNA structures decorated with cytoplasmic and granule proteins (Boeltz et al., 2019). Extensive NET release was found to have a disadvantageous proinflammatory and prothrombotic effect in various diseases (Jiménez-Alcázar et al., 2017; Sørensen and Borregaard, 2016). The importance of neutrophils and neutrophil-derived particles is illustrated by genetic defects. For example, inherited malfunction of neutrophil adhesion molecules (leukocyte adhesion deficiency syndromes) results in higher susceptibility to infection, because neutrophils poorly arrest and fail to reach pathogens (Ley et al., 2018). Patients with inherited degranulation malfunctions suffer from recurrent infections due to reduced antibacterial compound release (Ley et al., 2018).

Here, we report the discovery of a novel neutrophil-derived microparticle type, elongated neutrophil-derived structures (ENDS). ENDS derive from rolling neutrophils and contain the damage-associated molecular pattern S100A8–S100A9 complex. We describe ENDS formation, morphology, and molecular composition. We demonstrate that degrading ENDS release S100A8–S100A9 complex and that the number of ENDS is greatly increased in blood plasma of LPS-injected mice and septic patients.

Results and discussion

Mechanism of ENDS formation

We imaged in vivo neutrophil rolling in the mouse cremaster vasculature. In this model, the surgical preparation provides sufficient trauma to initiate neutrophil rolling and adhesion in venules (Kunkel et al., 1997). To increase neutrophil rolling and arrest, we induced the expression of endothelial E-selectin via an intrascrotal injection of TNF-α 2 h before imaging (Kunkel et al., 1997). To clearly demarcate the neutrophil plasma membrane, we injected Ly6G-AF647 antibody (Marki et al., 2018). This method reveals neutrophil tethers, which are not visible in vivo without fluorescent membrane labeling.

Slower-rolling neutrophils formed tethers that detached at the tether anchor point (where the tether is attached to the endothelial substrate; Sundd et al., 2012). However, some of the tether-forming neutrophils rolled at a faster rate, and their tethers broke along their length, sometimes multiple times, to form ENDS (Fig. 1, A and B; Video 1; and Video 2). In a venule with an estimated wall shear stress (WSS) of 9.6 dyn/cm², 4 of 69 rolling neutrophils (∼6%) formed 9 ENDS during 144 s (∼4 ENDS formed per minute; Video 2). In 27 venules of eight mice, 233 ENDS were visible, 81% of which remained immobile on the endothelium and 19% seemed to be sliding along the vessel wall (Fig. S1 A and Video 3). The median length of ENDS was 7 µm (2–112 µm); examples are shown in Fig. 1 C. 24% of ENDS showed a thicker, bead-like structure, typically at one end (Fig. 1 C and Fig. S1 B). ENDS were detectable in the circulation by intravital microscopy (Fig. S1 C) and in blood plasma isolated from mice after cremaster intravital microscopy (Fig. S1 D). These findings suggest that ENDS produced by rolling neutrophils in vivo can detach and appear in plasma.

To test whether human neutrophils can form ENDS, we imaged rolling of CD16-AF647 antibody–labeled human neutrophils on P-selectin or E-selectin substrates in flow chambers. We set the coating concentration to match the neutrophil rolling speed observed in mice in vivo, and we controlled the WSS with a syringe pump. Human neutrophils rolling on E-selectin at 40 dyn/cm² formed copious numbers of ENDS (Fig. 1 D). To investigate the dependence of ENDS formation on WSS, we developed an image-processing algorithm to segment ENDS and distinguish them from tethers, the structures still attached to neutrophils (Fig. 1 E and Video 4). We ramped up WSS in 10 dyn/cm² increments every 2 min. On both P- and E-selectin, ENDS started forming above 30 dyn/cm² and the formation accelerated with increasing WSS (Fig. 1 F, bottom). Equivalent experiments conducted on murine neutrophils showed similar results (Fig. 1 F). To test whether ENDS formation happens in the absence of antibody labeling of neutrophils, we rolled unlabeled human neutrophils under similar conditions, and after the neutrophils detached from the substrate, we perfused the flow chamber with CD16-AF647 antibody, revealing many ENDS (Fig. S1 E). Thus, ENDS formation is not antibody induced.

To study the mechanism of ENDS release into plasma, we coated the first half, but not the second half, of a flow chamber with P-selectin. After depositing ENDS on the P-selectin–coated surface, we increased shear stress. ENDS showed sliding behavior, similar to that observed in mice in vivo. When they reached the selectin-free part of the flow chamber, ENDS immediately detached (Fig. 1 G). In vivo, selectin expression is highest in venules <50 µm (Runnels et al., 2006; Norman et al., 2003). Thus, ENDS in vivo will eventually reach a selectin-poor endothelium, probably in a larger venule or small vein, and detach. During intravital microscopy, we observed several examples of sliding ENDS detaching from the vessel wall (Video 3). Both in vivo and in flow chambers, ENDS can become very long (maximal length of 112 and 423 µm, respectively; Fig. S1 F).

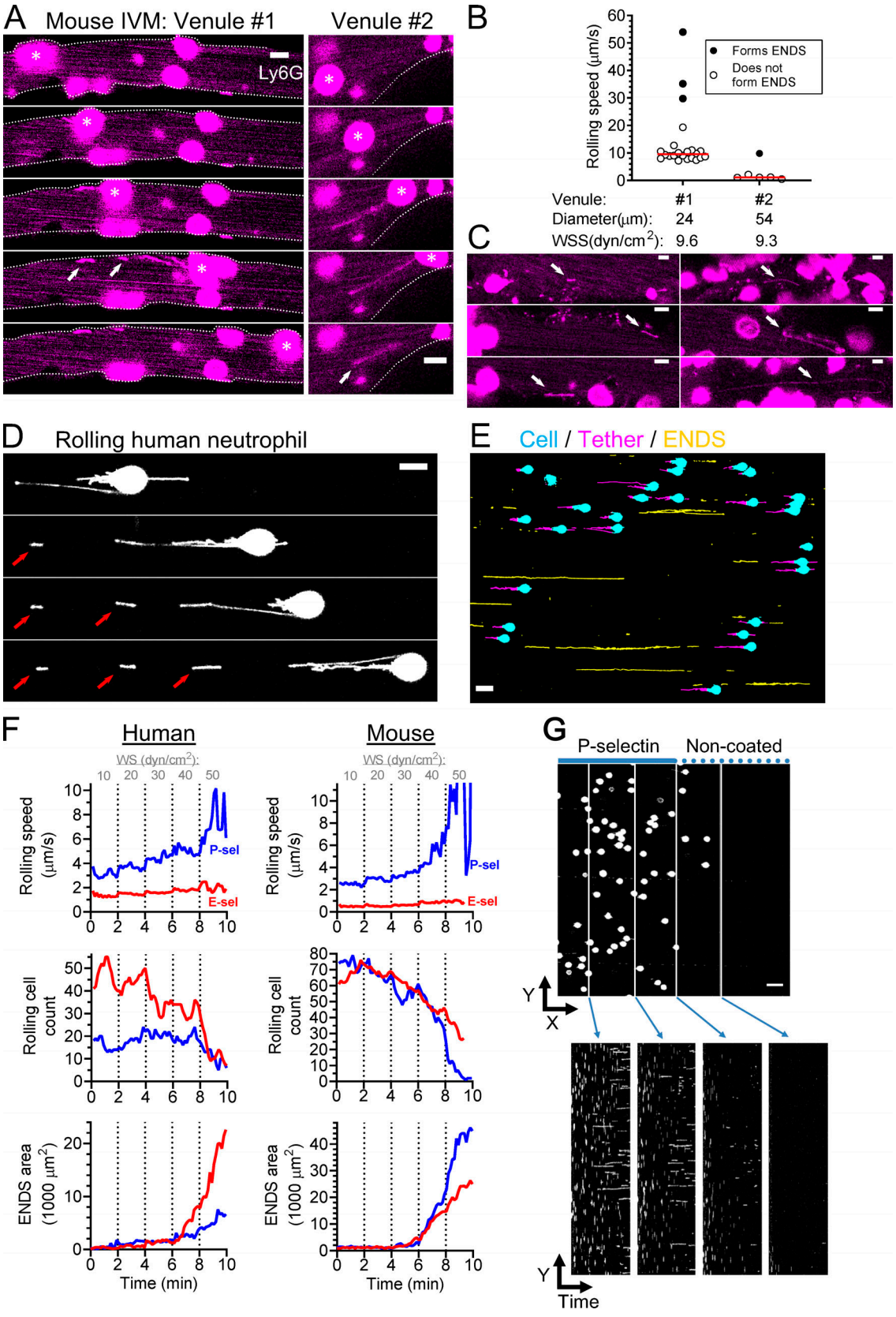

Figure 1. **Rolling neutrophils form ENDS. (A)** Consecutive frames of rolling neutrophils in cremaster venules of mice. Before intravital microscopy (IVM), the mice were intrascrotally injected with TNF-α to stimulate neutrophil interaction with the vasculature. Neutrophils were labeled via i.v. injection of Ly6G-AF647 antibody. Blood flow is from left to right. Asterisks indicate ENDS-forming neutrophils, and arrows point to ENDS. Dotted lines indicate the venule wall. Scale bar, 8 µm. **(B)** Analysis of neutrophil rolling speed and WSS in the venules shown in A. ENDS-forming neutrophils (indicated with full symbols) had the highest

rolling velocity in both examples. Red lines indicate median values. **(C)** ENDS (indicated by arrows) of various lengths observed in cremaster venules. Mice were pretreated as described above. Scale bars, 6 µm. **(D)** Human neutrophil labeled with CD16-AF647 forms ENDS while rolling on E-selectin substrate at 40 dyn/cm^2 WSS. Arrows indicate ENDS. Scale bar, 10 µm. **(E)** Image segmentation was developed to quantify ENDS formation in records of neutrophils rolling on E-selectin substrate. Cell body is color coded with cyan, tethers that are still attached to the cell are magenta, and ENDS that are not attached to the cell are yellow. Scale bar, 20 µm. **(F)** Human or mouse neutrophils rolled on P-selectin (blue curve) or E-selectin (red curve) substrate at increasing WSS. Surface area covered by ENDS to quantify ENDS formation. One representative example of three experiments is shown. **(G)** Rolling mouse neutrophils were allowed to form ENDS in a flow chamber. Only the upstream half was coated with P-selectin; the downstream half was uncoated. Neutrophils and sliding ENDS detached as they reached the noncoated half of the chamber. Upper panel shows a snapshot of rolling neutrophils and sliding ENDS. Lower panel shows kymograph analyses that were done in the positions indicated by the white lines on the upper panel. Scale bar, 50 µm. One representative example of two independent experiments is shown.

Our rolling experiments show that ENDS are preferentially released by fast-rolling neutrophils that show unstable rolling with jumps compared with non-ENDS-forming neutrophils in the same vessel. This suggests that the ENDS formation mechanism involves tether failure, because tethers, the precursors of ENDS, are load-bearing structures, and upon tether breakage, the rolling neutrophil shows a short acceleration (Marki et al., 2016, 2018; Ramachandran et al., 2004; Sundd et al., 2012). The number of tethers per neutrophil increases with increasing shear stress, suggesting that tethers stabilize neutrophil rolling (Ramachandran et al., 2004; Sundd et al., 2012; Marki et al., 2016, 2018). Various studies support the view that tether growth requires flow of plasma membrane into the tethers (Simunovic et al., 2017; Pospieszalska and Ley, 2009). This suggests that in stably rolling neutrophils, the tether growth rate keeps up with the rolling velocity (Marki et al., 2016, 2018). However, in unstably rolling neutrophils, the membrane supply cannot keep up with the tether-pulling rate. If the tether is strongly anchored to the substrate, the tether breaks between the cell and the anchor point. Another possibility could be that tether separation from the rolling neutrophil is mediated by an active molecular mechanism that could sever the tether.

ENDS morphology and molecular composition

To obtain high-resolution images of human ENDS, we isolated CD16-AF647–labeled ENDS from flow chambers, fixed them on a cover glass, and performed correlative confocal and scanning EM (SEM; Fig. 2 A and Fig. S1 A). By SEM, ENDS showed an apparent diameter of 77 ± 14 nm (average ± SD, n = 5). By comparing neutrophil diameter measured by SEM and by live confocal microscopy, we estimated the fixation-induced sample shrinkage to be 30%, which is in agreement with another report (Sundd et al., 2012). Thus, we estimate the true ENDS diameter to be ∼110 nm. The bead-like structures observed by confocal microscopy were resolved as branched, curled structures of unknown molecular composition by SEM (Fig. 2 A). To measure ENDS diameter with an alternative method, we measured human CD16-AF647 surface-labeled ENDS with stochastic optical reconstruction microscopy (STORM) superresolution microscopy. We measured five ENDS from two independent experiments (Fig. 2 B) by CD16 spot distribution across the cross section of ENDS (Fig. 2 C). Based on full width at half maximum, we found the average diameter of ENDS to be 115 nm, in excellent agreement with our SEM measurements.

Next, we investigated whether ENDS contain organelles. To this end, we produced human ENDS from neutrophils that were labeled for their surface with CD16-AF647 antibody and for different intracellular organelles. Labeling with CellTracker Orange CMRA, Mito Tracker Green, ER Tracker Green, or Hoechst showed that cytoplasm, mitochondria, ER, or DNA were readily labeled in neutrophils (positive control). ENDS only stained for cytoplasm (Fig. 2 D). We conclude that ENDS contain cytoplasm, but not mitochondria, ER, or DNA.

To investigate the molecular composition of ENDS, we used liquid chromatography–tandem mass spectrometry (LC-MS/MS) for an unbiased overview of the ENDS proteome. We generated ENDS in a flow chamber via rolling isolated human neutrophils. To minimize neutrophil contamination of the ENDS samples, we used low calcium (Ca^{2+}/Mg^{2+}-free PBS). Under these conditions, neutrophils cannot arrest but still form tethers by binding to P-selectin (coated at a higher density). The proteomes of three ENDS samples from different healthy donors were compared with the same amount of protein isolated from neutrophils. The total number of peptide spectrum matches (PSMs) detected in these samples showed modest variation (PSM count = 3,357 ± 336 [average ± SD]), showing that similar amounts of protein from each sample were analyzed. In ENDS, we identified 79 proteins (based on two or more PSMs and present in at least two of the three ENDS samples; Table 1 and Table S1). The 10 most abundant proteins in ENDS, which we also detected in similar amounts in whole neutrophil lysates, were lactotransferrin, albumin, actin (cytoplasmic 1), myeloperoxidase, S100A8, S100A9, α-enolase, GAPDH, annexin-A3, and catalase.

Lactotransferrin, myeloperoxidase, and albumin can be found in neutrophil granules (Rørvig et al., 2013), suggesting that ENDS may contain granules; however, by comparing the ENDS proteome to published proteomic datasets, we found that ENDS are more similar to neutrophil EVs (Timár et al., 2013) and NETs (Petretto et al., 2019) than to neutrophil granules (Rørvig et al., 2013) or neutrophil plasma membrane (Rørvig et al., 2013; Fig. S2 B). This appears to be in accordance with the ENDS formation mechanism, as ENDS are pinched off from the cell surface. Similar to ectosomes, they contain plasma membrane and cytosolic components. However, while ectosome formation requires assembly of molecular complexes at the plasma membrane, tethers, the precursors of ENDS, are pulled out from the plasma membrane. Adhesion molecules that anchor tethers are concentrated on the tips of microvilli (Bruehl et al., 1997). Most of the proteins common between ENDS and EVs belonged to the regulated exocytosis pathway. However, only ENDS contained certain proteins of the myeloid leukocyte activation and glycolytic metabolism pathways (Table S1). Thus, the molecular composition of ENDS is similar, but not identical, to EVs.

In neutrophils, we identified a similar number of proteins (76) as in ENDS (two or more PSMs; Table S1). Of these, 45 were

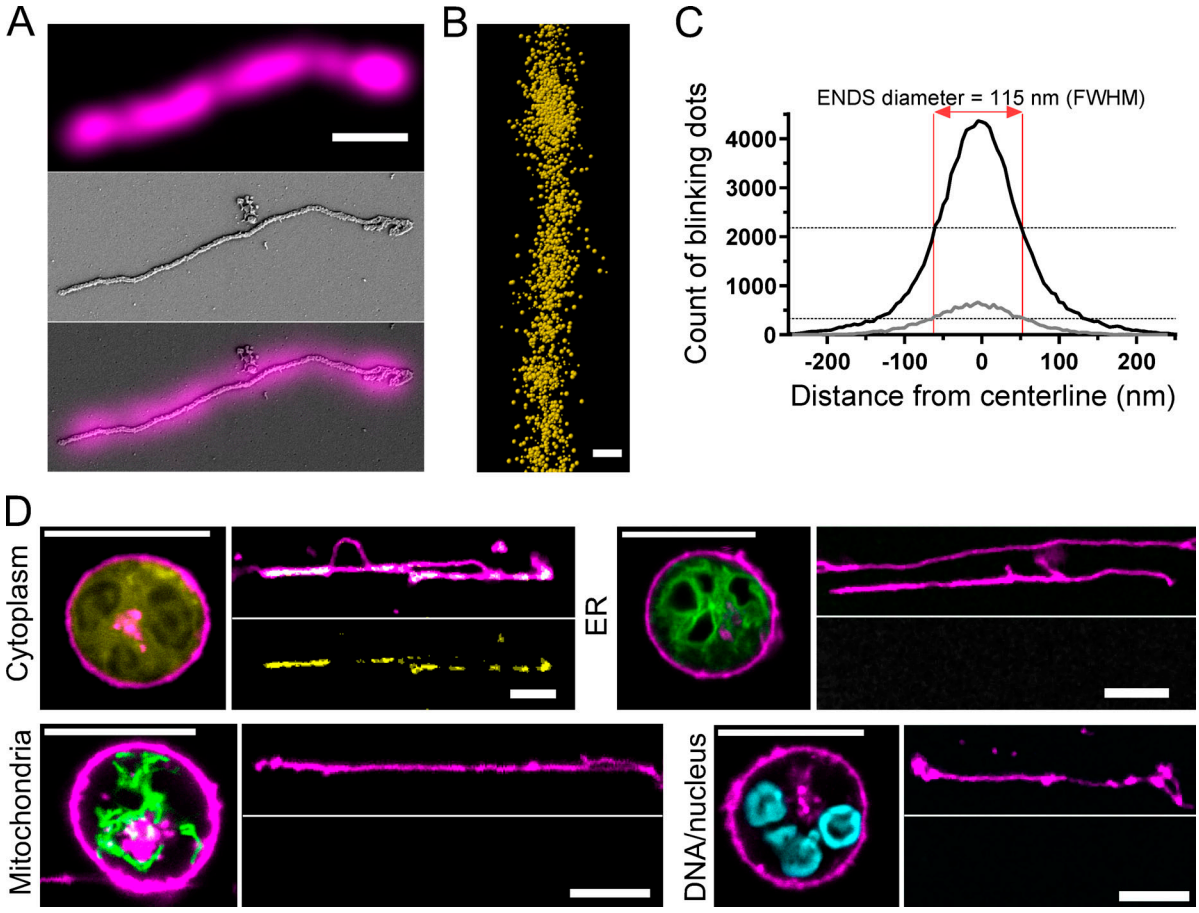

Figure 2. **Structure and composition of human ENDS. (A)** SEM and confocal image of ENDS formed on P-selectin substrate by human neutrophils surface labeled with CD16-AF647 antibody (magenta). Scale bar, 1 µm. **(B)** ENDS formed on E-selectin labeled with CD16-AF647 antibody were analyzed with STORM. Image shows a section of ENDS. Dots indicate the localization of the labeling antibody detected with STORM. Certainty of localization ≤20 nm. Scale bar, 100 nm. **(C)** The frequency histogram shows the distribution of CD16-AF647 labeling antibody across the width of ENDS measured as in B. Data were collected from two independent experiments (black and gray curves). The distance between the vertical red lines indicates mean ENDS diameter determined as the full width at half maximum (FWHM) value. Bin size is 5 nm. **(D)** To test the presence of organelles in ENDS, neutrophils were labeled for their surface (CD16-AF647 antibody, magenta), cytoplasm (CellTracker Orange CMRA, yellow), ER (ER Tracker Green), mitochondria (Mito Tracker Green), or nucleus/DNA (Hoechst, cyan) and rolled on E-selectin substrate. Only the cytoplasm tracer was detectable in ENDS formed by these neutrophils. Scale bars, 10 µm. Each of the experiments shown on this figure were repeated at least twice.

present in both ENDS and neutrophils, and 31 were detected only in neutrophils. To obtain an overview of the pathways covered by the ENDS proteome, we conducted gene ontology analysis using Metascape and found that the leukocyte degranulation pathway was highly represented in ENDS (Fig. S2 C). On the other hand, in the neutrophil proteome, we found regulated exocytosis, humoral immune response, and phagocytosis to be highly enriched pathways (Fig. S2 C).

Degrading ENDS round up and release S100A8–S100A9 complex

In flow chamber experiments, we observed that ENDS were long, elongated structures immediately after formation, but contracted and rounded up over the next 4 h in Ca^{2+}/Mg^{2+} HBSS buffer at room temperature (Fig. 3 A). In some instances, we observed fragmentation of ENDS as well. Contracted ENDS had a twofold smaller surface area and significantly increased sphericity (Fig. 3 B). The initial elongated shape of ENDS is a consequence of their formation mechanism described above. Similar elongated microparticles of erythrocyte or platelet origin were detected with cryo-EM in EV isolates of healthy human blood (Yuana et al., 2013; Arraud et al., 2014). It is not clear how these structures maintain their elongated shape. Our observation suggest that ENDS can stay elongated for a limited time but eventually round up within a few hours after formation.

To test whether degrading ENDS lose their membrane integrity, we measured intracellular free calcium in ENDS labeled with the Ca^{2+} reporter dye Fluo4-AM. In fresh ENDS, intracellular free calcium concentration was low and greatly increased after exposure to ionomycin (Fig. 3 C), indicating that fresh ENDS were able to keep calcium out. ENDS stained with Fluo4-AM after 7-h incubation did not respond significantly to ionomycin (Fig. 3 C), suggesting that ENDS lose their membrane integrity over time. To test whether they release the abundant cytosolic protein S100A8–S100A9 complex, we prepared ENDS in a flow chamber and imaged the entire chamber and counted

Table 1. **Proteome of human ENDS**

		PSM				PSM				PSM	
	Protein	ENDS	PMN		Protein	ENDS	PMN		Protein	ENDS	PMN
1	LTF	68	58	28	TALDO1	7	—	55	CORO1A	3	2
2	ALB	50	151	29	GSN	6	3	56	APOD	3	4
3	ACTB	36	38	30	AZGP1	6	8	57	ANXA6	3	—
4	MPO	35	32	31	IGHG1	6	20	58	GLIPR2	3	—
5	S100A9	34	16	32	PPIA	6	—	59	ITGAM	3	—
6	S100A8	27	3	33	HSPA8	6	2	60	PGAM1	3	2
7	ENO1	19	7	34	TGM3	6	3	61	GYG1	3	—
8	GAPDH	18	3	35	HP	5	13	62	IGHA1	3	10
9	ANXA3	18	4	36	ALDOA	5	—	63	ITGB2	3	—
10	CAT	16	4	37	ARHGDIB	5	2	64	P4HB	3	—
11	PGD	16	3	38	MYH9	5	5	65	PRDX6	3	—
12	PGK1	15	3	39	HIST1H4A	5	15	66	S100A7	3	—
13	ANXA1	15	10	40	PNP	5	—	67	SERPINB12	3	—
14	ACTN1	15	2	41	JUP	5	—	68	PRDX2	3	—
15	LCP1	13	5	42	YWHAZ	5	—	69	SERPINB4	2	2
16	LCN2	12	6	43	SERPINB1	5	2	70	ACTC1	3	3
17	GPI	10	—	44	PFN1	5	3	71	HIST1H2AB	2	7
18	TPI1	10	—	45	CTSG	5	6	72	CA2	2	—
19	LDHA	9	—	46	COL1A1	5	—	73	RAP1B	2	—
20	TKT	8	—	47	LDHB	5	—	74	HSPA5	2	2
21	TNF	8	50	48	MSN	5	—	75	PRTN3	2	3
22	GNAI2	8	—	49	PKM	4	2	76	HIST2HBF	2	7
23	CA1	7	—	50	GSTP1	4	4	77	ARG1	2	—
24	HSPA1B	7	—	51	CTSD	4	2	78	HK3	2	—
25	MMP9	7	2	52	DEFA1	4	9	79	MUCL1	2	—
26	HRNR	7	8	53	PGLYRP1	4	—				
27	LTA4H	7	—	54	BASP1	4	—				

LC/MS-MS spectrometry was performed on ENDS and neutrophil lysates. Each imaging experiment was performed independently at least twice. PSM values of the detected proteins are shown. The proteins indicated in red cells were detected only in the ENDS samples. The remainder of the proteins were detected in both ENDS and polymorphonuclear neutrophils (PMN).

the ENDS. Following 1-h incubation during confocal scanning and 7- and 24-h incubation in a tissue culture incubator, ENDS supernatants contained increasing amounts of S100A8–S100A9 complex (Fig. 3 D). Our ENDS preparations contained a few contaminating neutrophils that did not detach during washing. To account for this, we corrected the supernatant S100A8–S100A9 complex for the count of contaminating neutrophils. The normalized data show that ENDS released at least four times more S100A8–S100A9 than neutrophils.

Blood from septic mice and patients contains increased number of ENDS, fragmented ENDS, and S100A8–S100A9 complex

Sepsis is known to be associated with strong neutrophil activation in blood (Sônego et al., 2016). Thus, we reasoned that the number of ENDS might be elevated during sepsis. To test this hypothesis in an experimental model, we treated wild-type mice by i.p. injection of high-dose LPS of *Escherichia coli* (O5:B55 strain, 40 mg/kg; Soromou et al., 2014; Napier et al., 2019). With imaging cytometry, we detected 730 ± 199 ENDS/µl of plasma (average ± SD) at 2 h after LPS (Fig. 4 A) but no ENDS in plasma of control mice. To avoid any possible artifacts due to labeling with antibodies, we performed this experiment on Ly6G-cre-mT/mG mice (Muzumdar et al., 2007; Hasenberg et al., 2015) that expressed plasma membrane–anchored EGFP in neutrophils only. We bled the same mice before and 2 h after LPS injection, isolated blood plasma, and observed the ENDS count by confocal microscopy. Before LPS injection, we detected no ENDS in the blood plasma; however, 2 h after LPS injection, we detected 1.1 ± 0.2 ENDS per field of view

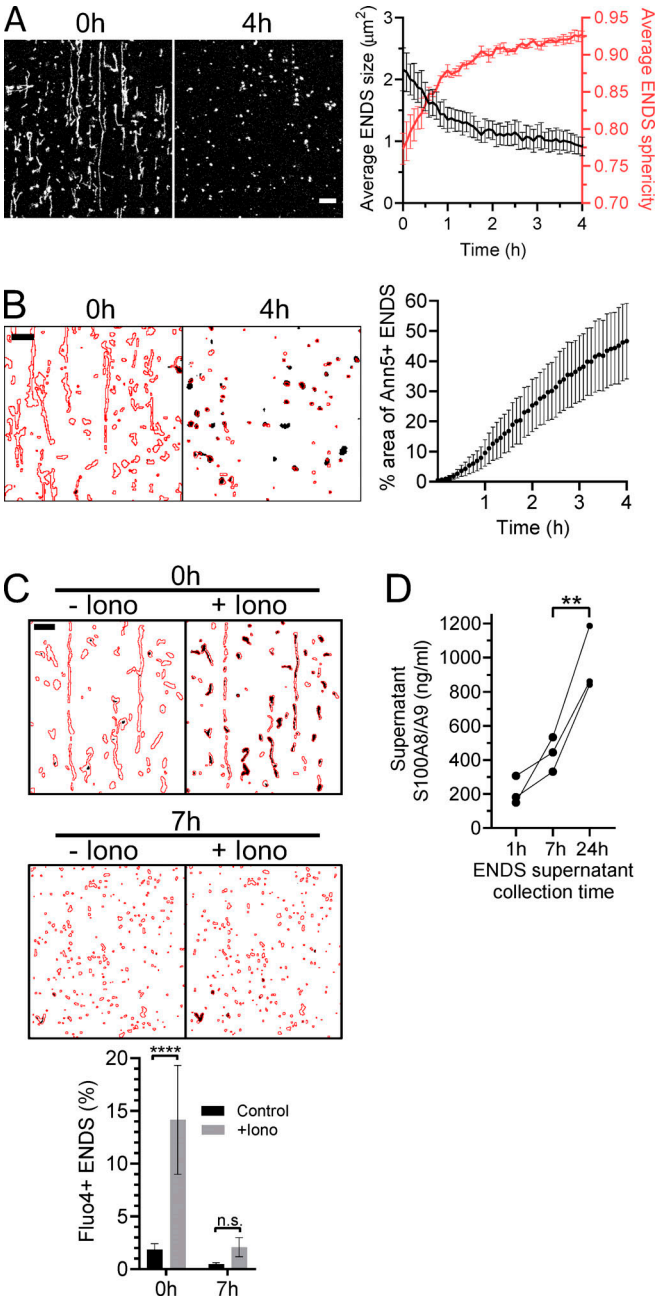

Figure 3. **ENDS degrade and release S100A8–S100A9 complex.** ENDS were produced from human neutrophils on an E-selectin–coated substrate as shown in Fig. 1. **(A)** ENDS were surface labeled with CD16-AF647 antibody and imaged over 4 h. During that period, ENDS contracted as indicated by their decreasing size (area; black line) and increasing sphericity (red line). Values represent average ± SEM of three independent experiments. **(B)** Human ENDS were imaged over 4 h in the presence of fluorescently labeled annexin-5 (Ann5) in the incubation buffer. The red outlines indicate the ENDS contours determined based on surface labeling with CD16-AF647 antibody. Black pixels show the thresholded annexin-5 signal. After 4-h incubation, ~50% of ENDS were annexin-5 positive. Average ± SEM of three independent experiments. **(C)** Fresh (0-h-old) and 7-h-old human ENDS were loaded with Fluo4-AM to measure intraluminal free Ca^{2+} before and after exposure to ionomycin (Iono). The red outlines indicate the ENDS contours indicated by CD16-AF647 surface labeling. Black pixels indicate the thresholded Fluo4 signal. Values represent average ± SEM of seven independent experiments. Statistical analysis was done using a paired *t* test; ****, P < 0.0001. **(D)** S100A8–S100A9 complex concentrations were measured in supernatants of ENDS produced with human neutrophils in a flow chamber. ENDS were incubated in HBSS buffer for 1, 7, or 24 h. Statistical analysis was performed using a ratio paired *t* test; **, P = 0.0096. Scale bars, 10 µm.

(average ± SD; Fig. S2 D). Example images of these ENDS are shown in Fig. 4 B.

For quantitative analysis of ENDS and EVs in septic human blood, we used imaging flow cytometry on blood plasma from 12 septic patients and 7 healthy controls (Table S2). We used CD16 and CD66b as neutrophil markers, which were also present on human ENDS formed in a flow chamber (Fig. S2 E). Septic blood samples contained ~100 times more neutrophil-derived $CD16^+$ and $CD66b^+$ microparticles (120,000 ± 32,000/µl [septic] versus 1,100 ± 200/µl [healthy; average ± SEM]; Fig. 4 C). With the same scanning technique, Headland et al. (2014) reported 100 neutrophil-derived EVs/µl healthy human blood plasma. The difference between these results could be explained by different plasma preparation protocols (Chandler, 2016). Headland et al. (2014) centrifuged the blood once at 300 *g* for 5 min and then at 10,000 *g* for 2 min. We centrifuged the blood once at 1,000 *g* for 5 min. Likely, centrifugation at higher *g* force may have removed some EVs from Headland et al.'s samples.

The dominant neutrophil-derived particle populations in healthy blood samples were negative for TSs and PS (50 ± 8% [average ± SEM]). The second-largest fraction was positive for TSs but negative for PS (40 ± 7%; Fig. 4 D). This distribution shifted in the septic samples, where the TS- and PS-negative particles became more abundant (72 ± 5%) at the expense of the TS-positive particles (17 ± 3%). Among TS and PS double-negative particles, ENDS with an aspect ratio <0.6 (considered elongated) accounted for 3.1 ± 1.2% in septic and 2.5 ± 1.6% in healthy individuals (average ± SEM; Fig. 4 E). Based on our microfluidic flow chamber studies, we know that the spherical (aspect ratio >0.6) objects double negative for TS and PS are most likely fragmented ENDS, because in vitro ENDS round up and fragment over time; after 4-h incubation, 40% of the degraded ENDS remain PS negative, and only few ENDS stain for TSs (Fig. S2 F). However, we do not have direct in vivo evidence for fragmentation. Example images of ENDS and fragmented ENDS captured with ImageStream are shown in Fig. 4 F. With confocal microscopy, we could confirm the presence of CD16-AF647–stained ENDS in septic plasma (Fig. 4 G). The septic samples contained on average ~100-fold more ENDS (elongated only, all double negative for TSs and PS) compared with control plasma (595 ± 159/µl [septic] versus 5 ± 4/µl [healthy]; Fig. 4 H). The median length of the 1,277 ENDS that we detected in plasma of the 12 septic samples was 6 µm (range, 4–28.5 µm).

The ENDS count in septic plasma positively correlated with blood neutrophil counts (Fig. 4 I). In the septic samples, plasma S100A8–S100A9 complex levels significantly and positively correlated with fragmented ENDS, but not with intact ENDS counts (Fig. 4 J). Taken together with our in vitro observation that ENDS degrade over time and release S100A8–S100A9 complex, this suggests that degrading ENDS are a likely source of free extracellular S100A8–S100A9 complex in septic plasma.

Proteins S100A8 and S100A9, also known as MRP-8 and MRP-14 or calgranulin A and B (Pruenster et al., 2016), were

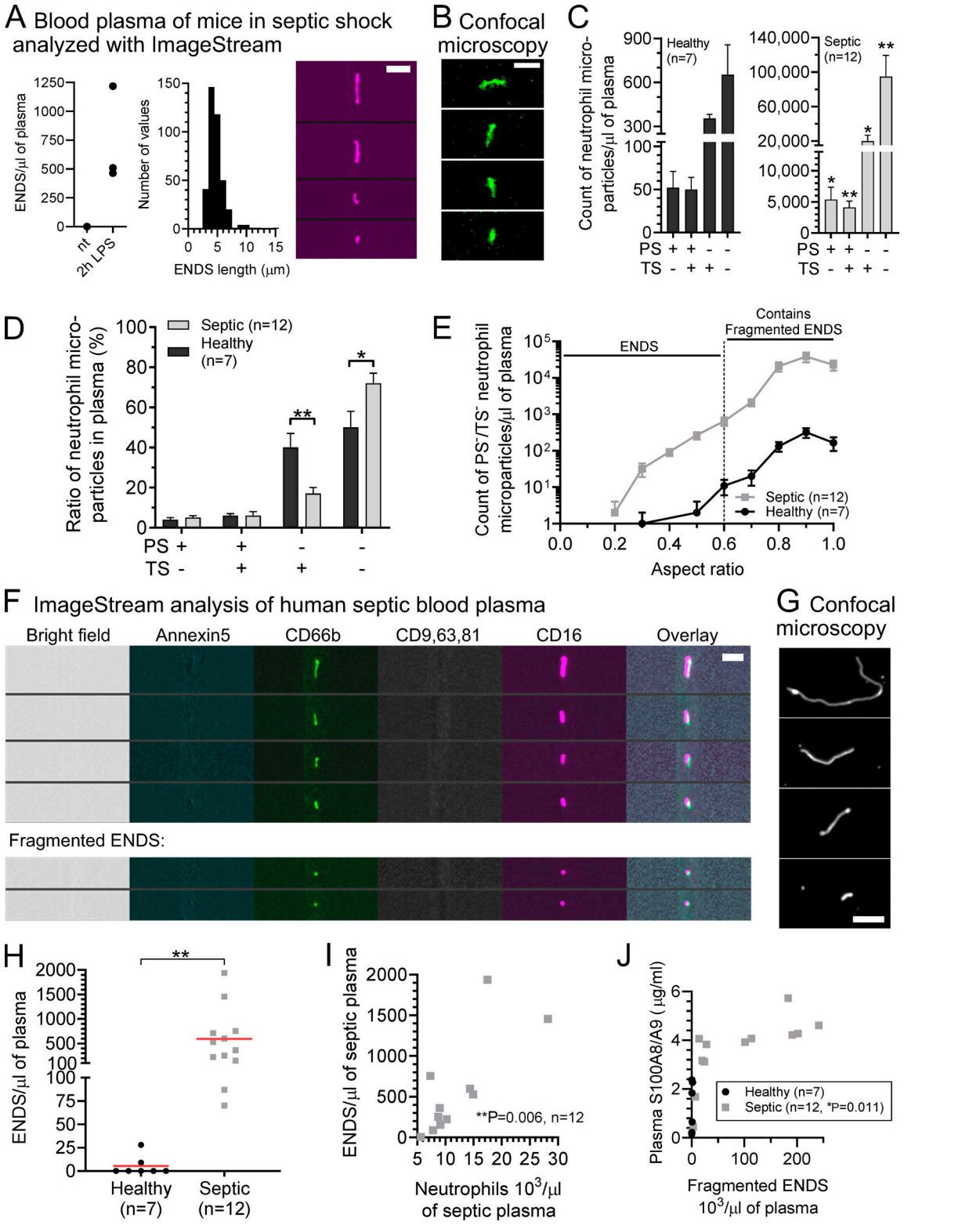

Figure 4. **Blood plasma contains elevated number of ENDS during sepsis. (A)** Three mice each were injected i.p. with LPS (40 mg/kg) or PBS (not treated, nt). Retro-orbital blood was collected at 2 h, and plasma was prepared by centrifuging at 1,000 *g* for 5 min. Fluorescently labeled anti-Ly6G antibody was added, and samples were scanned with ImageStream. The images show examples of Ly6G antibody–stained ENDS. Scale bar, 10 µm. **(B)** Confocal images show examples of EGFP-labeled ENDS, detected in the blood plasma of Ly6G-cre-mT/mG mice harvested 2 h after i.p. LPS injection. Scale bar, 5 µm. **(C and D)** Count (C) and ratio (D) of neutrophil-derived ($CD66b^+$ and $CD16^+$) micro objects detected with ImageStream in healthy (black) and septic (gray) human plasma. Micro objects were labeled for TSs with PE-labeled CD9, CD63, and CD81 antibodies and for PS with annexin-5-eF450. Septic plasma samples contained significantly more micro objects with each marker combination (average and SEM are shown; two-tailed *t* test with Welch's correction, from left to right: *, P = 0.0251; **, P = 0.029; *, P = 0.0184; **, P = 0.039). In septic samples the ratio of TS^-/PS^- objects was increased at the expense of the TS^+/PS^- objects (two-tailed *t* test: *, P = 0.0123; **, P =

0.003). **(E)** Aspect ratio (width/length ratio) of TS^- and PS^- neutrophil-derived micro objects in septic and healthy plasma. Objects with an aspect ratio <0.6 were considered ENDS, and objects with an aspect ratio >0.6 were considered to contain fragmented ENDS. **(F)** Examples of ENDS and fragmented ENDS detected with ImageStream in septic blood are shown. Each lane represents a different object, and each column represents a channel of a different marker. Scale bar is 10 µm. **(G)** Confocal images confirm the presence of $CD16^+$ elongated structures in septic plasma labeled with CD16-AF647 antibody. Numbers indicate ENDS length (in micrometers). Scale bar, 5 µm. **(H)** ENDS content of healthy and septic blood plasma are shown. Red lines indicate average values. Statistical analysis: two-tailed *T* test with Welch's correction, **, P = 0.0045. **(I)** ENDS count showed linear correlation with neutrophil counts. Statistical analysis was done using a correlation analysis and two-tailed test; **, P = 0.006. **(J)** In septic, but not healthy, samples, the plasma S100A8–S100A9 complex concentration correlated with fragmented ENDS count. Statistical analysis was done using a correlation analysis and two-tailed test; *, P = 0.011. n.s., not significant.

among the most abundant proteins in ENDS (Table 1). These proteins are abundant in neutrophil cytosol, where they form heterodimers that buffer Ca^{2+} and regulate microtubule formation (Pruenster et al., 2016). Neutrophils release S100A8–S100A9 complexes following activation or during NETs release or necrosis (Pruenster et al., 2016). Outside of the cell, S100A8–S100A9 can bind TLR4 and elicit several effects. S100A8–S100A9 can activate immune cells (Ehrchen et al., 2009), but it can also induce endotoxin tolerance upon prolonged exposure (Austermann et al., 2014). In the presence of calcium, S100A8–S100A9 complexes form tetramers $(S100A8–S100A9)_2$ and lose their TLR4 binding affinity (Vogl et al., 2018). The S100A8–S100A9 complex is increased in the blood of septic or trauma patients (Austermann et al., 2014; Simm et al., 2016).

We found that degrading ENDS release S100A8–S100A9 into their environment. Our experiments show that ENDS initially maintain a low luminal calcium level and respond to ionomycin, suggesting that ENDS can keep calcium out and, at least for some time, can keep the S100A8–S100A9 complexes in. As long as S100A8–S100A9 complexes are in a low-calcium environment, they remain dimers that retain the ability to bind TLR4. This is reminiscent of migrating neutrophils in extravascular tissue, which were found to release LTB4 packaged into EVs (Majumdar et al., 2016) that extend the half-life of LTB4 and enable coordination of neutrophil swarming. Similarly, in the lungs of chronic obstructive pulmonary disease patients, neutrophil elastase is released on the surface of neutrophil-derived exosomes, which prevents neutrophil elastase inhibition by α-antitripsin (Genschmer et al., 2019). In virally infected trachea tissue of mice, migrasomes formed by migrating neutrophils gradually released CXCL12 over time, which formed a chemokine trail behind the neutrophil that guides the migration of lymphocytes (Lim et al., 2015).

Conclusion

Here, we report the discovery of ENDS, which are a new type of neutrophil-derived microparticle. ENDS form when tethers detach from rolling neutrophils. ENDS are initially elongated. Over time, they fragment and round up. Unlike the known neutrophil-derived EVs, ENDS do not express TSs and do not bind annexin-5. ENDS also differ from migrasomes, because ENDS form in the vessel lumen from microvilli of nonpolarized rolling neutrophils, whereas migrasomes form in the extravascular space from the uropod of polarized migrating neutrophils. Human blood plasma ENDS counts are increased ∼100-fold in sepsis. The ENDS fragment count positively correlates with the concentration of S100A8–S100A9 complex in septic blood.

Materials and methods

Intravital microscopy

The experimental animal procedures of this study were performed in accordance with guidelines approved by the Institutional Animal Care and Use Committee of La Jolla Institute (LJI) for Allergy and Immunology, which is an American Association for Accreditation of Laboratory Animal Care accredited facility. Cremaster intravital microscopy was performed on male C57BL/6J mice ≥8 wk as described earlier (Marki et al., 2018). Approximately 3 h before imaging, mice were administered an intrascrotal injection with 500 ng TNF (PeproTech) in 300 µl PBS. The femoral artery was cannulated with a PE-10 tube, and the cremaster muscle was exteriorized for imaging with a resonant scanner confocal microscope (Leica SP8; Leica Microsystems). To label the neutrophil surface, 10 min before imaging, 5 µl (2.5 µg) anti-Ly6G-Alexa Fluor 647 monoclonal antibody (1A8; BioLegend) was injected in 100 µl PBS via the femoral artery. To measure WSS, 0.5-µm fluorescent spheres (Spherotech) were injected via a femoral artery catheter, and the vessel was imaged at a high frame rate to resolve the displacement of the fastest beads. WSS was calculated with the following formula: $WSS = (0.625 \times 8 \times 2.2 \times v_{max}/\text{diameter}) \times \eta$, where the maximum flow velocity (v_{max}) was calculated from the fastest bead frame-to-frame displacement, vessel diameter was measured on transillumination images, and mouse blood plasma viscosity (η) at 37°C was estimated by another study (Windberger et al., 2003) to be 0.013 s × dyn/cm². At the end of the imaging session, blood was collected from the femoral artery catheter into a heparinized syringe. Plasma isolated via centrifugation at 1,000 *g* for 5 min was loaded into an ibidi flow chamber (#80161; ibidi) and scanned for the presence of ENDS with a Leica SP8 confocal microscope equipped with a resonant scanner and hybrid detectors through a Leica 25×/0.95 NA water-immersion objective (Leica Microsystems).

Neutrophil rolling in a flow chamber

Human neutrophils were isolated with Polymorphoprep (Alere Technologies) from healthy donors of the LJI normal blood donation program. Human neutrophils (10^6) were labeled for 10 min in 100 µl Ca^{2+}/Mg^{2+} containing HBSS (GIBCO BRL, Thermo Fisher Scientific) supplemented with 1 µl (0.2 µg) anti-CD16-Alexa Fluor 647 antibody (3G8; BioLegend). Mouse neutrophils were isolated from the bone marrow of C57BL/6J mice ≥8 wk into Ca^{2+}/Mg^{2+} containing HBSS. The isolate was filtered through a 40-µm nylon strainer (Biopioneer), mouse neutrophils (10^6) were labeled for 10 min in 100 µl Ca^{2+}/Mg^{2+} HBSS with 1 µl (0.5 µg) anti-Ly6G-AF647 antibody. ibidi flow chambers (#80161) were coated for 15 min with 1 µg/ml recombinant

human or mouse P- or E-selectin-Fc chimera (R&D Systems) and blocked for 30 min with casein blocking solution (Thermo Fisher Scientific). A 10-ml syringe without a piston connected to the inflow orifice of the flow chamber was used as an inflow reservoir, and a 60-ml syringe connected to the outflow orifice was used to generate flow via suction with a syringe pump (PhD2000; Harvard Apparatus). 100 µl labeled neutrophil suspension was loaded into the flow chamber at the inflow point, and a gentle (0.1 ml/min) flow was applied to bring the cells into contact with the substrate. Once neutrophils covered the entire substrate, a perfusion ramp programed into the pump was started, and the cells were perfused with Ca^{2+}/Mg^{2+} HBSS as follows (each perfusion lasted for 2 min): 1.9 ml/min (10 dyn/cm^2), 3.8 ml/min (20 dyn/cm^2), 5.7 ml/min (30 dyn/cm^2), 7.6 ml/min (40 dyn/cm^2), and 9.5 ml/min (50 dyn/cm^2). Neutrophils were imaged during the perfusion with Zeiss LSM880 confocal microscope in Airyscan through 20× air 0.8 NA objective (Carl Zeiss Microscopy).

To analyze the records, a segmentation method was developed with Imaris 8.3 (Bitplane) and Fiji (Rueden et al., 2017; Schindelin et al., 2012; http://fiji.sc/) software. For quantification of ENDS formation, the raw records were surface modeled and the objects that were in connection with neutrophils were excluded based on their width. The dataset was cleaned up manually frame-by-frame via omitting the signals of fly-by and partially detected cells. The remaining objects were assumed to be ENDS. Eventually, count and total surface area of ENDS were measured. To analyze neutrophil rolling speed and count, a cell body mask was created with Fiji. "MinError" threshold and 1-pixel median filter were applied on the images. The outermost pixels of the objects were eroded to remove the masks of small or thin objects and then dilated with a few pixels to completely cover the cell body. This cell body mask was loaded into Imaris and, with the spot tracking function, the rolling speed and cell count were measured. To segment tethers, the raw record was surface modeled, and objects not in contact with neutrophils were omitted based on their width. From the resulting "neutrophil with tether" mask, the cell body mask was subtracted.

Correlative SEM

ENDS produced by human neutrophils were harvested from a flow chamber with Trypsin-EDTA (0.05%, 5 min). ENDS suspension was spun at 1,000 *g* in a swinging bucket centrifuge onto a graded coverglass taped to a 35-mm dish with a hole in the middle (MatTek dish without the central cover glass). Samples were fixed for 15 min with 1.5% glutaraldehyde in PBS and dehydrated in increasing concentrations of ethanol. ENDS were imaged by confocal microscopy (20× air 0.8 NA objective, LSM880; Carl Zeiss Microscopy). The cover glass was removed from the dish, critical point dried and heavy metal coated (Zhang et al., 2012), and imaged with Zeiss Sigma500 scanning electron microscope (Carl Zeiss Microscopy). The ENDS detected with confocal microscopy were located with SEM based on the grids. Fiji was used to align and overlay the confocal and SEM images.

STORM imaging

Human neutrophils were isolated from blood of healthy donors as described above. One million human neutrophils were incubated for 10 min in 100 µl Ca^{2+}/Mg^{2+}-free PBS supplemented with 2 µl (1 µg) anti-CD18 antibody (clone 1B4; BioLegend) to block β2-integrins and prevent neutrophil arrest and 1 µl (0.2 µg) CD16-AF647 antibody to label neutrophil surface. The cells were rolled in an ibidi flow chamber (#80607, coated with 0.1 µg/ml human recombinant E-selectin and blocked with casein) under 50–100 dyn/cm^2 shear stress generated with perfusion of HBSS containing Ca^{2+}/Mg^{2+}. This resulted in ENDS formation and detachment of the vast majority of neutrophils. The ENDS were fixed via incubation of the chamber lumen for 1 h with 1.5% glutaraldehyde (EMS) PBS solution.

Chambers were washed with PBS and filled with STORM blinking buffer that was made freshly before application via mixing 890 µl buffer B (50 mM Tris, pH 8.0, 10 mM NaCl, and 10% glucose), 100 µl MEA buffer (1 M MEA [#30070; Sigma-Aldrich] in 0.25 N HCl), and 10 µl GLOX buffer (56 U/ml glucose oxidase [#G2133; Sigma-Aldrich], 340 U/ml catalase [#C40; Sigma-Aldrich], 10 mM Tris, pH 8.0, and 50 mM NaCl). Samples were imaged on a Nikon Ti microscope equipped with Nikon oil-immersion 1.49 NA 100× Apo total internal reflection microscopy fluorescence objective (Nikon Instruments) and an Andor Ixon3 Ultra DU897 electron multiplying couple-charged device camera (Oxford Instruments). Illumination angle was set to 80° and frame size was set to 256 × 256 pixels in the center of the field of view. After acquisition of a reference total internal reflection fluorescence microscopy image, the 647-nm laser output power was increased to induce blinking. 20,000 frames were collected over 12 min.

The x and y coordinates and lateral localization accuracy of the blinking spots were extracted with the Nikon STORM software. The obtained dataset was loaded into Imaris with the "Super Resolution Localization Data to Spot" function. Spots that clearly localized outside of ENDS and/or had lateral localization precision >20 nm were omitted. The remaining spots were converted into an image. Images of straight segments of each detected ENDS were imported into Fiji to find the rotation angle needed to align them to the y axis. The coordinates of the spots from each segment were then imported into MATLAB and rotated by the calculated angle using an affine transform. The segments were divided along the vertical y axis into 100-nm sections. In each section, the range of the x coordinates was calculated, and the localizations were shifted to center at 0 using the following formula: $x_{centered} = x - x_{min} - (x_{max} - x_{min})/2$. The normalized x coordinates of localizations in all ENDS were plotted on a frequency histogram with a 5-nm bin size. The width at half maximum of this histogram was measured to determine the average diameter of ENDS.

Confocal imaging for presence of organelles

Human neutrophils were isolated from blood of healthy donors as described above. One million human neutrophils were incubated for 15 min in 100 µl Ca^{2+}/Mg^{2+}-free PBS supplemented with 1:1,000 CMRA, 5:10,000 Mito Tracker Green, and 5:10,000 ER Tracker Green (Thermo Fisher Scientific). Suspension was diluted with Ca^{2+}/Mg^{2+}-free PBS to 500 µl and centrifuged for 5 min at 400 *g*. Cells were resuspended in 100 µl Ca^{2+}/Mg^{2+}-free PBS supplemented with 2 µl (1 µg) anti-CD18 antibody (clone

1B4; BioLegend) to block β2-integrins and prevent neutrophil arrest and 1 µl (0.2 µg) CD16-AF647 antibody to label neutrophil surface. After 10 min, the cells were rolled in an ibidi flow chamber (#80161, coated with 0.5 µg/ml human recombinant E-selectin and blocked with casein) under 50–100 dyn/cm^2 shear stress generated with perfusion of HBSS containing Ca^{2+}/Mg^{2+}. The perfusion was stopped before the last cells would detach from the substrate. For DNA imaging, after rolling, Hoechst 33342 (Thermo Fisher Scientific) diluted 1:1,000 in PBS was added into the flow chamber. Neutrophils and ENDS were imaged immediately without fixation on a Zeiss LSM 880 microscope with 20× air (NA = 0.8) or 63× oil-immersion (NA = 1.4) objective. Images were processed with Fiji software. Median filter 1 was applied, and the dynamic range was adjusted to omit the background signal.

Proteomics analysis

To examine the protein composition, ENDS were produced in a flow chamber system as described above with minor modifications. Isolated human neutrophils were rolled in a P-selectin–coated ibidi flow chamber in Ca^{2+}/Mg^{2+}-free PBS. Lack of Ca^{2+} and Mg^{2+} prevented integrin-mediated neutrophil arrest but still allowed selectin mediated rolling, although at lower efficacy. To compensate for this, the flow chamber coating density was increased via coating with 10 µg/ml recombinant human P-selectin–Fc-chimera. Following application of a 4-min-long shear stress (ramp to 100 dyn/cm^2), the neutrophils formed ENDS and detached from the substrate. ENDS were isolated from the flow chamber via perfusion with 0.5 mM EDTA and 10 s of vortexing. For each donor, ENDS isolate of three flow chambers were pooled together. The suspension was centrifuged at 400 *g* for 5 min to minimize any neutrophil contamination, and the supernatants were concentrated to ∼30 µl with an Amicon Ultra 0.5 ml 10k filter unit (Millipore-Sigma). The ENDS were lysed for 1 h at 4°C by adding RIPA lysis and extraction buffer (Thermo Fisher Scientific) supplemented with PMSF protease inhibitor (Thermo Fisher Scientific) and cOmplete protease inhibitor cocktail (Sigma-Aldrich) and stored at −20°C.

The proteomes of five samples (ENDS from donors 1–3, neutrophils from donor 3, and a coated empty chamber as background control) were determined using LC/MS-MS proteomics at the Systems Mass Spectrometry Core at the Georgia Institute of Technology. Proteins were digested as described (Wiśniewski et al., 2009) and analyzed by high-pressure nano-LC-MS/MS as previously described (Naing et al., 2018) with the following modifications. Trypsin was used as the protease, and the spectral dataset was analyzed with Mascot using a UniProt Reference Proteome database (downloaded on January 7, 2018, with 20,416 entries) combined with a database containing common laboratory contaminants (www.thegpm.org/cRAP). Following removal of common laboratory contaminants (e.g., keratin) and exogenously added proteins (e.g., trypsin from the digestion, P-selectin and BSA used in coating the plates), and hemoglobin, the total numbers of PSMs were used as crude estimates for relative abundance in subsequent analysis. The background PSM value was subtracted from the PSM value of each detected protein. Proteins, which had more than one PSM ≤0 out of the three donor values, were excluded from further analysis. The PSM values of the three donors were averaged, and proteins with an average of two or fewer PSMs were omitted from further analysis. Gene names were rendered to the detected proteins, and gene ontology analysis was performed with Metascape (http://metascape.org). The ENDS proteome was compared with published datasets of neutrophil-derived EVs (Timár et al., 2013), NETs (Petretto et al., 2019), and neutrophil granule and plasma membrane (Rørvig et al., 2013) proteomes by rendering gene names to every protein and dataset overlap analysis with Venny (Oliveros, 2007). Similarities were quantified via calculating the Jaccard similarity index based on the following formula: JSI = 100 × (count of shared proteins / count of shared and unshared proteins).

Fragmentation and permeability test

For the fragmentation test, 10^6 human neutrophils were incubated for 10 min in 100 µl Ca^{2+}/Mg^{2+} HBSS supplemented with blocking anti-CD18 antibody (clone 1B4; BioLegend) to block β2-integrins and prevent neutrophil arrest. The cells were rolled in an ibidi flow chamber (coated with 0.5 µg/ml human recombinant E-selectin-Fc chimera and blocked with casein) under 150 dyn/cm^2 shear stress generated with HBSS containing Ca^{2+}/Mg^{2+}. This resulted in ENDS formation and detachment of the vast majority of neutrophils. To label the ENDS, the chamber was incubated for 10 min with 100 µl Ca^{2+}/Mg^{2+} HBSS supplemented with 1 µl CD16-AF647 antibody. Without washing out the antibody, every 5 min, confocal images of the ENDS were captured for 4 h. The records were analyzed in Fiji by applying "triangle" threshold and 1-pixel median filter and measuring the object count and total surface area covered by ENDS. For the permeability test, two chambers of ENDS were prepared shortly after each other in the same way as described above. One of the chambers was stained with Fluo4 (30-min incubation with 5 µM Fluo4) immediately and was imaged for CD16-AF647 and Fluo4 while being perfused with 14 µM ionomycin. 7 h later, the other chamber was labeled and imaged in the same way. Records were analyzed with Fiji, triangle threshold and 1-pixel median filter were applied on the images, a mask was created from the CD16-AF647 signal, and the Fluo4$^+$ surface area was measured within that mask.

Measurement of S100A8–S100A9 complex release by ENDS

ENDS were prepared in the same way as for the fragmentation test (see above). To measure the neutrophil contamination of the ENDS samples and estimate ENDS quantity, the entire flow chamber was scanned in tile/z-stack mode with a confocal microscope (Zeiss LSM880 through 10× air objective; Fig. S1 E). The flow chamber filled with Ca^{2+}/Mg^{2+} HBSS was placed into a tissue culture incubator. After 7 h, the chamber was washed through with 100 µl Ca^{2+}/Mg^{2+} HBSS, and the effluent was collected. After 24 h, the supernatant was harvested via pressing air into the chamber with a syringe. The collected supernatants were immediately centrifuged at 22,000 *g* for 10 min and two 50-µl aliquots of each sample were placed at −80°C. To measure the S100A8–S100A9 released by whole neutrophils, we loaded with 10^4 human neutrophils in 100 µl Ca^{2+}/Mg^{2+} HBSS into wells

of a 96-well plate coated with E-selectin and blocked with casein similarly to the flow chambers. After a 24-h incubation in a tissue culture incubator, the supernatant was collected and processed in the same way as the ENDS supernatants. S100A8 and S100A9 levels were measured by ELISA following the manufacturer instructions (BioLegend). The z-stack/tile scan images of the CD16-AF647–labeled chambers were analyzed with Fiji. Z-stacks were collapsed with maximum projection and were processed with threshold "Yen" and median filter 2. Objects with area between 50 and 150 μm^2 were counted as single cells. Objects with area >150 μm^2 were considered as clusters of neutrophils, and their area was divided with the average single-cell area, which was 86, 80, and 82 μm^2 for the three samples.

ENDS detection in mice with septic shock

Mice were injected i.p. with 40 mg/kg LPS (*E. coli*, strain O55:B5; Sigma-Aldrich) that was dissolved in sterile PBS at 10 mg/ml concentration. This treatment induces severe septic shock to which the mice succumb within 24 h (Soromou et al., 2014).

For ENDS detection with antibody labeling and imaging cytometry, 33 noninjected and LPS-injected and 2-h incubated ∼4-mo-old wild-type C57BL/6J female mice were bled retro-orbitally. 70 µl blood was mixed with 70 µl PBS supplemented with heparin at 2%. 50 µl blood plasma isolated by 5-min centrifugation at 1,000 *g* was supplemented with 1 µl heparin and 0.5 µl (0.25 µg) Ly6G-FITC and Ly6G-AF647 antibodies (clone 1A8; BioLegend). After 15-min incubation at room temperature in the dark, 4 µl the suspension was added to 96 µl annexin-5 binding buffer, and the resulting 50-times-diluted plasma sample was loaded into a round-bottom 96-well plate for scanning with ImageStream (Amnis ImageStream X Mark II; Luminex). Please note that analyzing 50-times-diluted plasma can interfere with the hydrodynamic focusing of ImageStream and may result in unsuccessful experiments in which the stream of plasma does not pass under the detection zone. Each sample was analyzed for 20 min with ImageStream with a 40× objective at highest sensitivity, lowest speed, core flow diameter 6 µm, automatic bead removal and maximum laser powers. The records were analyzed with the IDEAS (Luminex). The compensation matrix was created based on healthy blood plasma of healthy mice stained with one antibody at the time. "Fill" mask was applied on each fluorescent channel. Flow speed gate 66–67 was applied to eliminate objects artificially elongated (smeared) by unstable flow. Events with a bright-field area signal >5 μm^2 were excluded from the analysis. Fluorescently labeled antibodies tend to aggregate in suspension; on ImageStream records, the resulting clumps have an appearance similar to EVs. To avoid counting antibody clumps as false-positive counts, only objects positive for Ly6G-FITC and Ly6G-AF647 were taken as neutrophil derived. Single-spot count gate was applied on the detected channels to exclude events with multiple objects in the field of view. ENDS were gated as objects with aspect ratio and length in the FITC channel >0.65 and 3 µm. ENDS concentration measured by ImageStream was multiplied by 50 to account for the plasma dilution.

For antibody-free ENDS detection with confocal scanning, mice with neutrophils expressing plasma membrane–targeted EGFP (Ly6G-cre-mT/mG mice) were bred by crossing a strain carrying mT/mG genetic construct (Muzumdar et al., 2007) with a strain carrying Cre-recombinase in the Ly6G locus (Hasenberg et al., 2015). The first-generation heterozygous offspring were used for the experiments. Three female littermate Ly6G-EGFP mice of almost 11 mo of age were bled retro-orbitally before and 2 h after LPS injection. During bleeding, the mice were anesthetized with isoflurane inhalation, and 35 µl blood was collected into a heparin-coated glass capillary. To prevent blood clot formation, the blood was mixed with 35 µl PBS containing 2% of sterile heparin stock (#504036; Fresenius Kabi). The blood was centrifuged for 5 min at 1,000 *g*, and 30 µl blood plasma was collected and loaded into an ibidi flow chamber (#80626; ibidi) and was scanned with the Leica SP8 confocal microscope equipped with a resonant scanner and 40× oil-immersion objective. With the LAS Navigator, an overview tile scan was captured with the Spiral function, 30 fields of view were randomly marked, and each field of view was manually scanned in XYT mode (settings: 1,024 × 128, 1.5 zoom, 3–4 Airy unit aperture, 8× line average, and 633 laser power at 20%). The representative images were filtered with median 1.

ENDS and S100A8–S100A9 complex detection in human plasma

Human blood samples were collected under protocols approved by LJI and University of California, San Diego institutional review boards (IRBs). Healthy human blood samples were obtained from LJI normal blood donation program (IRB numbers VD-057 and BHR1-KL). Septic human blood specimens were obtained from the University of California, San Diego clinical laboratory (IRB number 130973X; "Identifying immune correlates of disease processes"). Patients were selected based on SIRS criteria (two or more of the following: hypo- or hyperthermia, tachycardia, hyperventilation, leukocytosis, or leukopenia; Singer et al., 2016) and diagnosis of infection upon hospitalization. Blood was drawn into EDTA vacutainers and stored for up to 3 d at 4°C without agitation. Blood plasma was isolated via centrifugation at 1,000 *g* for 5 min. Several 50 µl aliquots were frozen at −80°C for S100A8–S100A9 complex analysis. For confocal imaging, 50 µl of the plasma was supplemented with 1 µl anti-CD16-AF647 antibody. After a 15-min incubation at room temperature in the dark, the suspension was spun into the glass of MatTek dishes, and the sample was scanned with Zeiss780 confocal microscope through a 40× oil-immersion 1.3 NA objective (Carl Zeiss Microscopy). For scanning with ImageStream, 25 µl plasma was supplemented with 1 µl heparin, 24 µl annexin-5 binding buffer, 5 µl annexin-5-eFluor450 (Thermo Fisher Scientific), 2.5 µl (0.5 µg) anti-CD66b-FITC (G10F5), and 1 µl anti-CD9-PE (20 ng, HI9a), anti-CD63-PE (100 ng, H5C6), anti-CD81-PE (200 ng, 5A6), and anti-CD16-AF647 antibodies (BioLegend). After 30-min incubation at room temperature, the mixture was diluted 50-fold in annexin-5 binding buffer (123-fold final dilution of plasma) and loaded into a 96-well plate for automatic scanning. Data were acquired with a 40× objective at highest sensitivity, lowest speed, core flow diameter 6 µm, automatic bead removal, and maximum laser powers. The records were analyzed with the IDEAS

(Luminex). Fill mask was applied on each fluorescent channel. Flow speed gate 66–67 was applied to eliminate objects artificially elongated (smeared) by unstable flow. Objects with bright-field area >8 μm² were excluded from analysis. Single-spot count gate was applied on the detected channels to exclude events with multiple objects in the field of view. To avoid false-positive counts due to antibody clumps, the neutrophil-derived objects were gated as objects double positive for CD66b and CD16. ENDS were gated as $CD66b^+CD16^+[CD9,63,81]^-$annexin-$5^-$ population, aspect ratio (CD16) <0.6, and area (CD16) >4. Fragmented ENDS were gated as $CD66b^+CD16^+[CD9,63,81]^-$annexin-$5^-$ population, aspect ratio (CD16) >0.6. The ENDS populations were manually cleaned up for events with multiple objects in the field of view. Object counts and ENDS length values were exported for further analysis. S100A8–S100A9 contents of the healthy and septic plasma samples were measured with S100A8–S100A9 ELISA (BioLegend). Before measurement, the plasma aliquots were centrifuged for 10 min at 18,000 *g*, and the supernatant was diluted 40 times.

Statistical analysis

Paired or unpaired two-tailed *t* tests with or without Welch's correction and correlation analyses were performed in Prism software. Significance values are indicated in the figure legends (*, $P \le 0.05$; **, $P \le 0.001$).

Online supplemental material

Fig. S1 shows that rolling neutrophils form ENDS. Fig. S2 shows the ultrastructure and composition of ENDS. Video 1 shows ENDS formation in vivo. Video 2 shows the formation of multiple ENDS in the same vessel in vivo. Video 3 shows ENDS sliding and detaching from the venular wall in vivo. Video 4 shows ENDS formation in a flow chamber. Table S1 shows ENDS proteome analysis. Table S2 lists clinical data of septic patients.

Acknowledgments

We are thankful to Dr. Erzsebet Ligeti for her valuable suggestion on the experimental designs.

The Ley laboratory was supported by National Institutes of Health program project grants P01 HL078784 and P01 HL151433. A. Marki was supported by an American Heart Association postdoctoral fellowship (17POST33410940) and the Tullie and Rickey Families SPARK Award at La Jolla Institute for Immunology. H. Winkels was supported by Deutsche Forschungsgemeinschaft award GZ WI 4811/1-1. M. Orecchioni was supported by an American Heart Association postdoctoral fellowship 18POST34060251. Z. Fan was supported by National Institutes of Health grant R01HL145454 and American Heart Association postdoctoral fellowship and career development awards 16POST31160014 and 18CDA34110426. The purchase of the Zeiss LSM 880 microscope was made possible by National Institutes of Health grant S10OD021831 awarded to the Microscopy Core Facility at the La Jolla Institute.

Author contributions: K. Ley, A. Marki, K. Buscher, and Z. Fan designed the experiments. A. Marki set up and performed most of the experiments. K. Buscher, C. Lorenzini, and M. Orecchioni performed flow cytometry and flow chamber experiments. M. Meyer prepared the samples for proteomic analysis. R. Saigusa performed the S100A8–S100A9 ELISA measurements. Y.-T. Yeh performed the SEM experiments. N. Hartmann did flow chamber experiments. G.J. Golden developed the septic mouse assay. J.M. Dan and J. Bui provided the septic blood samples. W.B. Kiosses performed STORM imaging. R. Ganesan, S. McArdle, and H. Winkels performed data analysis. Z. Mikulski provided microscopy expertise. Y. Altman provided ImageStream expertise. D. Smalley performed the proteomics analysis. J. Roth provided S100A8–S100A9 expertise. A. Marki, V. Nizet, and K. Ley wrote the manuscript. M. Kronenberg, S. Chien, J.D. Esko, and K. Ley financed the study. K. Ley supervised the study.

Disclosures: The authors declare no competing interests exist.

Submitted: 24 March 2020
Revised: 28 September 2020
Accepted: 6 November 2020

References

Arraud, N., R. Linares, S. Tan, C. Gounou, J.M. Pasquet, S. Mornet, and A.R. Brisson. 2014. Extracellular vesicles from blood plasma: determination of their morphology, size, phenotype and concentration. *J. Thromb. Haemost.* 12:614–627. https://doi.org/10.1111/jth.12554

Austermann, J., J. Friesenhagen, S.K. Fassl, B. Petersen, T. Ortkras, J. Burgmann, K. Barczyk-Kahlert, E. Faist, S. Zedler, S. Pirr, et al. 2014. Alarmins MRP8 and MRP14 induce stress tolerance in phagocytes under sterile inflammatory conditions. *Cell Rep.* 9:2112–2123. https://doi.org/10.1016/j.celrep.2014.11.020

Boeltz, S., P. Amini, H.J. Anders, F. Andrade, R. Bilyy, S. Chatfield, I. Cichon, D.M. Clancy, J. Desai, T. Dumych, et al. 2019. To NET or not to NET: current opinions and state of the science regarding the formation of neutrophil extracellular traps. *Cell Death Differ.* 26:395–408. https://doi.org/10.1038/s41418-018-0261-x

Bruehl, R.E., K.L. Moore, D.E. Lorant, N. Borregaard, G.A. Zimmerman, R.P. McEver, and D.F. Bainton. 1997. Leukocyte activation induces surface redistribution of P-selectin glycoprotein ligand-1. *J. Leukoc. Biol.* 61:489–499. https://doi.org/10.1002/jlb.61.4.489

Chandler, W.L. 2016. Measurement of microvesicle levels in human blood using flow cytometry. *Cytometry B Clin. Cytom.* 90:326–336. https://doi.org/10.1002/cyto.b.21343

Christoffersson, G., and M. Phillipson. 2018. The neutrophil: one cell on many missions or many cells with different agendas? *Cell Tissue Res.* 371:415–423. https://doi.org/10.1007/s00441-017-2780-z

Colombo, M., G. Raposo, and C. Théry. 2014. Biogenesis, secretion, and intercellular interactions of exosomes and other extracellular vesicles. *Annu. Rev. Cell Dev. Biol.* 30:255–289. https://doi.org/10.1146/annurev-cellbio-101512-122326

Colón, D.F., C.W. Wanderley, M. Franchin, C.M. Silva, C.H. Hiroki, F.V.S. Castanheira, P.B. Donate, A.H. Lopes, L.C. Volpon, S.K. Kavaguti, et al. 2019. Neutrophil extracellular traps (NETs) exacerbate severity of infant sepsis. *Crit. Care.* 23:113. https://doi.org/10.1186/s13054-019-2407-8

Dalli, J., T. Montero-Melendez, L.V. Norling, X. Yin, C. Hinds, D. Haskard, M. Mayr, and M. Perretti. 2013. Heterogeneity in neutrophil microparticles reveals distinct proteome and functional properties. *Mol. Cell. Proteomics.* 12:2205–2219. https://doi.org/10.1074/mcp.M113.028589

Ehrchen, J.M., C. Sunderkötter, D. Foell, T. Vogl, and J. Roth. 2009. The endogenous Toll-like receptor 4 agonist S100A8/S100A9 (calprotectin) as innate amplifier of infection, autoimmunity, and cancer. *J. Leukoc. Biol.* 86:557–566. https://doi.org/10.1189/jlb.1008647

Fine, N., O. Barzilay, C. Sun, N. Wellappuli, F. Tanwir, J.W. Chadwick, M. Oveisi, N. Tasevski, D. Prescott, M. Gargan, et al. 2019. Primed PMNs in healthy mouse and human circulation are first responders during acute inflammation. *Blood Adv.* 3:1622–1637. https://doi.org/10.1182/bloodadvances.2018030585

Genschmer, K.R., D.W. Russell, C. Lal, T. Szul, P.E. Bratcher, B.D. Noerager, M. Abdul Roda, X. Xu, G. Rezonzew, L. Viera, et al. 2019. Activated PMN Exosomes: Pathogenic Entities Causing Matrix Destruction and Disease in the Lung. *Cell.* 176:113–126.e15. https://doi.org/10.1016/j.cell.2018.12.002

Gómez-Moreno, D., J.M. Adrover, and A. Hidalgo. 2018. Neutrophils as effectors of vascular inflammation. *Eur. J. Clin. Invest.* 48(Suppl 2):e12940. https://doi.org/10.1111/eci.12940

Hasenberg, A., M. Hasenberg, L. Männ, F. Neumann, L. Borkenstein, M. Stecher, A. Kraus, D.R. Engel, A. Klingberg, P. Seddigh, et al. 2015. Catchup: a mouse model for imaging-based tracking and modulation of neutrophil granulocytes. *Nat. Methods.* 12:445–452. https://doi.org/10.1038/nmeth.3322

Headland, S.E., H.R. Jones, A.S. D'Sa, M. Perretti, and L.V. Norling. 2014. Cutting-edge analysis of extracellular microparticles using ImageStream(X) imaging flow cytometry. *Sci. Rep.* 4:5237. https://doi.org/10.1038/srep05237

Hong, C.W. 2018. Extracellular Vesicles of Neutrophils. *Immune Netw.* 18:e43. https://doi.org/10.4110/in.2018.18.e43

Hyun, Y.M., R. Sumagin, P.P. Sarangi, E. Lomakina, M.G. Overstreet, C.M. Baker, D.J. Fowell, R.E. Waugh, I.H. Sarelius, and M. Kim. 2012. Uropod elongation is a common final step in leukocyte extravasation through inflamed vessels. *J. Exp. Med.* 209:1349–1362. https://doi.org/10.1084/jem.20111426

Jiménez-Alcázar, M., C. Rangaswamy, R. Panda, J. Bitterling, Y.J. Simsek, A.T. Long, R. Bilyy, V. Krenn, C. Renné, T. Renné, et al. 2017. Host DNases prevent vascular occlusion by neutrophil extracellular traps. *Science.* 358:1202–1206. https://doi.org/10.1126/science.aam8897

Johnson, B.L. III, J.W. Kuethe, and C.C. Caldwell. 2014. Neutrophil derived microvesicles: emerging role of a key mediator to the immune response. *Endocr. Metab. Immune Disord. Drug Targets.* 14:210–217. https://doi.org/10.2174/1871530314666140722083717

Kunkel, E.J., U. Jung, and K. Ley. 1997. TNF-alpha induces selectin-mediated leukocyte rolling in mouse cremaster muscle arterioles. *Am. J. Physiol.* 272:H1391–H1400.

Ley, K., H.M. Hoffman, P. Kubes, M.A. Cassatella, A. Zychlinsky, C.C. Hedrick, and S.D. Catz. 2018. Neutrophils: New insights and open questions. *Sci. Immunol.* 3:eaat4579. https://doi.org/10.1126/sciimmunol.aat4579

Lim, K., Y.M. Hyun, K. Lambert-Emo, T. Capece, S. Bae, R. Miller, D.J. Topham, and M. Kim. 2015. Neutrophil trails guide influenza-specific CD8$^+$ T cells in the airways. *Science.* 349:aaa4352. https://doi.org/10.1126/science.aaa4352

Lőrincz, A.M., M. Schütte, C.I. Timár, D.S. Veres, Á. Kittel, K.R. McLeish, M.L. Merchant, and E. Ligeti. 2015. Functionally and morphologically distinct populations of extracellular vesicles produced by human neutrophilic granulocytes. *J. Leukoc. Biol.* 98:583–589. https://doi.org/10.1189/jlb.3VMA1014-514R

Maas, S.L.N., X.O. Breakefield, and A.M. Weaver. 2017. Extracellular Vesicles: Unique Intercellular Delivery Vehicles. *Trends Cell Biol.* 27:172–188. https://doi.org/10.1016/j.tcb.2016.11.003

Majumdar, R., A. Tavakoli Tameh, and C.A. Parent. 2016. Exosomes Mediate LTB4 Release during Neutrophil Chemotaxis. *PLoS Biol.* 14:e1002336. https://doi.org/10.1371/journal.pbio.1002336

Marki, A., E. Gutierrez, Z. Mikulski, A. Groisman, and K. Ley. 2016. Microfluidics-based side view flow chamber reveals tether-to-sling transition in rolling neutrophils. *Sci. Rep.* 6:28870. https://doi.org/10.1038/srep28870

Marki, A., K. Buscher, Z. Mikulski, A. Pries, and K. Ley. 2018. Rolling neutrophils form tethers and slings under physiologic conditions in vivo. *J. Leukoc. Biol.* 103:67–70.

Muzumdar, M.D., B. Tasic, K. Miyamichi, L. Li, and L. Luo. 2007. A global double-fluorescent Cre reporter mouse. *Genesis.* 45:593–605. https://doi.org/10.1002/dvg.20335

Naing, S.H., S. Kalyoncu, D.M. Smalley, H. Kim, X. Tao, J.B. George, A.P. Jonke, R.C. Oliver, V.S. Urban, M.P. Torres, and R.L. Lieberman. 2018. Both positional and chemical variables control *in vitro* proteolytic cleavage of a presenilin ortholog. *J. Biol. Chem.* 293:4653–4663. https://doi.org/10.1074/jbc.RA117.001436

Napier, B.A., M. Andres-Terre, L.M. Massis, A.J. Hryckowian, S.K. Higginbottom, K. Cumnock, K.M. Casey, B. Haileselassie, K.A. Lugo, D.S. Schneider, et al. 2019. Western diet regulates immune status and the response to LPS-driven sepsis independent of diet-associated microbiome. *Proc. Natl. Acad. Sci. USA.* 116:3688–3694. https://doi.org/10.1073/pnas.1814273116

Norman, M.U., N.C. Van De Velde, J.R. Timoshanko, A. Issekutz, and M.J. Hickey. 2003. Overlapping roles of endothelial selectins and vascular cell adhesion molecule-1 in immune complex-induced leukocyte recruitment in the cremasteric microvasculature. *Am. J. Pathol.* 163:1491–1503. https://doi.org/10.1016/S0002-9440(10)63506-7

Nourshargh, S., and R. Alon. 2014. Leukocyte migration into inflamed tissues. *Immunity.* 41:694–707. https://doi.org/10.1016/j.immuni.2014.10.008

Oliveros, J.C.V. 2007. An interactive tool for comparing lists with Venn's diagrams. https://bioinfogp.cnb.csic.es/tools/venny/index.html (accessed 2019).

Petretto, A., M. Bruschi, F. Pratesi, C. Croia, G. Candiano, G. Ghiggeri, and P. Migliorini. 2019. Neutrophil extracellular traps (NET) induced by different stimuli: A comparative proteomic analysis. *PLoS One.* 14:e0218946. https://doi.org/10.1371/journal.pone.0218946

Pospieszalska, M.K., and K. Ley. 2009. Dynamics of Microvillus Extension and Tether Formation in Rolling Leukocytes. *Cell. Mol. Bioeng.* 2:207–217. https://doi.org/10.1007/s12195-009-0063-9

Pruenster, M., T. Vogl, J. Roth, and M. Sperandio. 2016. S100A8/A9: From basic science to clinical application. *Pharmacol. Ther.* 167:120–131. https://doi.org/10.1016/j.pharmthera.2016.07.015

Ramachandran, V., M. Williams, T. Yago, D.W. Schmidtke, and R.P. McEver. 2004. Dynamic alterations of membrane tethers stabilize leukocyte rolling on P-selectin. *Proc. Natl. Acad. Sci. USA.* 101:13519–13524. https://doi.org/10.1073/pnas.0403608101

Rørvig, S., O. Østergaard, N.H. Heegaard, and N. Borregaard. 2013. Proteome profiling of human neutrophil granule subsets, secretory vesicles, and cell membrane: correlation with transcriptome profiling of neutrophil precursors. *J. Leukoc. Biol.* 94:711–721. https://doi.org/10.1189/jlb.1212619

Rueden, C.T., J. Schindelin, M.C. Hiner, B.E. DeZonia, A.E. Walter, E.T. Arena, and K.W. Eliceiri. 2017. ImageJ2: ImageJ for the next generation of scientific image data. *BMC Bioinformatics.* 18:529. https://doi.org/10.1186/s12859-017-1934-z

Runnels, J.M., P. Zamiri, J.A. Spencer, I. Veilleux, X. Wei, A. Bogdanov, and C.P. Lin. 2006. Imaging molecular expression on vascular endothelial cells by in vivo immunofluorescence microscopy. *Mol. Imaging.* 5:31–40. https://doi.org/10.2310/7290.2006.00004

Schindelin, J., I. Arganda-Carreras, E. Frise, V. Kaynig, M. Longair, T. Pietzsch, S. Preibisch, C. Rueden, S. Saalfeld, B. Schmid, et al. 2012. Fiji: an open-source platform for biological-image analysis. *Nat. Methods.* 9:676–682. https://doi.org/10.1038/nmeth.2019

Simm, M., E. Söderberg, A. Larsson, M. Castegren, T. Nilsen, M. Eriksson, and M. Lipcsey. 2016. Performance of plasma calprotectin as a biomarker of early sepsis: a pilot study. *Biomarkers Med.* 10:811–818. https://doi.org/10.2217/bmm-2016-0032

Simunovic, M., J.B. Manneville, H.F. Renard, E. Evergren, K. Raghunathan, D. Bhatia, A.K. Kenworthy, G.A. Voth, J. Prost, H.T. McMahon, et al. 2017. Friction Mediates Scission of Tubular Membranes Scaffolded by BAR Proteins. *Cell.* 170:172–184.e11. https://doi.org/10.1016/j.cell.2017.05.047

Singer, M., C.S. Deutschman, C.W. Seymour, M. Shankar-Hari, D. Annane, M. Bauer, R. Bellomo, G.R. Bernard, J.D. Chiche, C.M. Coopersmith, et al. 2016. The Third International Consensus Definitions for Sepsis and Septic Shock (Sepsis-3). *JAMA.* 315:801–810. https://doi.org/10.1001/jama.2016.0287

Soehnlein, O., S. Steffens, A. Hidalgo, and C. Weber. 2017. Neutrophils as protagonists and targets in chronic inflammation. *Nat. Rev. Immunol.* 17:248–261. https://doi.org/10.1038/nri.2017.10

Sônego, F., F.V. Castanheira, R.G. Ferreira, A. Kanashiro, C.A. Leite, D.C. Nascimento, D.F. Colón, V.F. Borges, J.C. Alves-Filho, and F.Q. Cunha. 2016. Paradoxical Roles of the Neutrophil in Sepsis: Protective and Deleterious. *Front. Immunol.* 7:155. https://doi.org/10.3389/fimmu.2016.00155

Sørensen, O.E., and N. Borregaard. 2016. Neutrophil extracellular traps - the dark side of neutrophils. *J. Clin. Invest.* 126:1612–1620. https://doi.org/10.1172/JCI84538

Soromou, L.W., L. Jiang, M. Wei, N. Chen, M. Huo, X. Chu, W. Zhong, Q. Wu, A. Baldé, X. Deng, and H. Feng. 2014. Protection of mice against lipopolysaccharide-induced endotoxic shock by pinocembrin is correlated with regulation of cytokine secretion. *J. Immunotoxicol.* 11:56–61. https://doi.org/10.3109/1547691X.2013.792886

Sundd, P., E. Gutierrez, E.K. Koltsova, Y. Kuwano, S. Fukuda, M.K. Pospieszalska, A. Groisman, and K. Ley. 2012. 'Slings' enable neutrophil rolling at high shear. *Nature.* 488:399–403. https://doi.org/10.1038/nature11248

Timár, C.I., A.M. Lorincz, R. Csépányi-Kömi, A. Vályi-Nagy, G. Nagy, E.I. Buzás, Z. Iványi, A. Kittel, D.W. Powell, K.R. McLeish, and E. Ligeti. 2013.

Antibacterial effect of microvesicles released from human neutrophilic granulocytes. *Blood.* 121:510–518. https://doi.org/10.1182/blood-2012-05-431114

van Niel, G., G. D'Angelo, and G. Raposo. 2018. Shedding light on the cell biology of extracellular vesicles. *Nat. Rev. Mol. Cell Biol.* 19:213–228. https://doi.org/10.1038/nrm.2017.125

Vogl, T., A. Stratis, V. Wixler, T. Völler, S. Thurainayagam, S.K. Jorch, S. Zenker, A. Dreiling, D. Chakraborty, M. Fröhling, et al. 2018. Auto-inhibitory regulation of S100A8/S100A9 alarmin activity locally restricts sterile inflammation. *J. Clin. Invest.* 128:1852–1866. https://doi.org/10.1172/JCI89867

Windberger, U., A. Bartholovitsch, R. Plasenzotti, K.J. Korak, and G. Heinze. 2003. Whole blood viscosity, plasma viscosity and erythrocyte aggregation in nine mammalian species: reference values and comparison of data. *Exp. Physiol.* 88:431–440. https://doi.org/10.1113/eph8802496

Wiśniewski, J.R., A. Zougman, N. Nagaraj, and M. Mann. 2009. Universal sample preparation method for proteome analysis. *Nat. Methods.* 6:359–362. https://doi.org/10.1038/nmeth.1322

Yuana, Y., R.I. Koning, M.E. Kuil, P.C. Rensen, A.J. Koster, R.M. Bertina, and S. Osanto. 2013. Cryo-electron microscopy of extracellular vesicles in fresh plasma. *J. Extracell. Vesicles.* 2:21494. https://doi.org/10.3402/jev.v2i0.21494

Zhang, A.P., X. Qu, P. Soman, K.C. Hribar, J.W. Lee, S. Chen, and S. He. 2012. Rapid fabrication of complex 3D extracellular microenvironments by dynamic optical projection stereolithography. *Adv. Mater.* 24:4266–4270. https://doi.org/10.1002/adma.201202024

Supplemental material

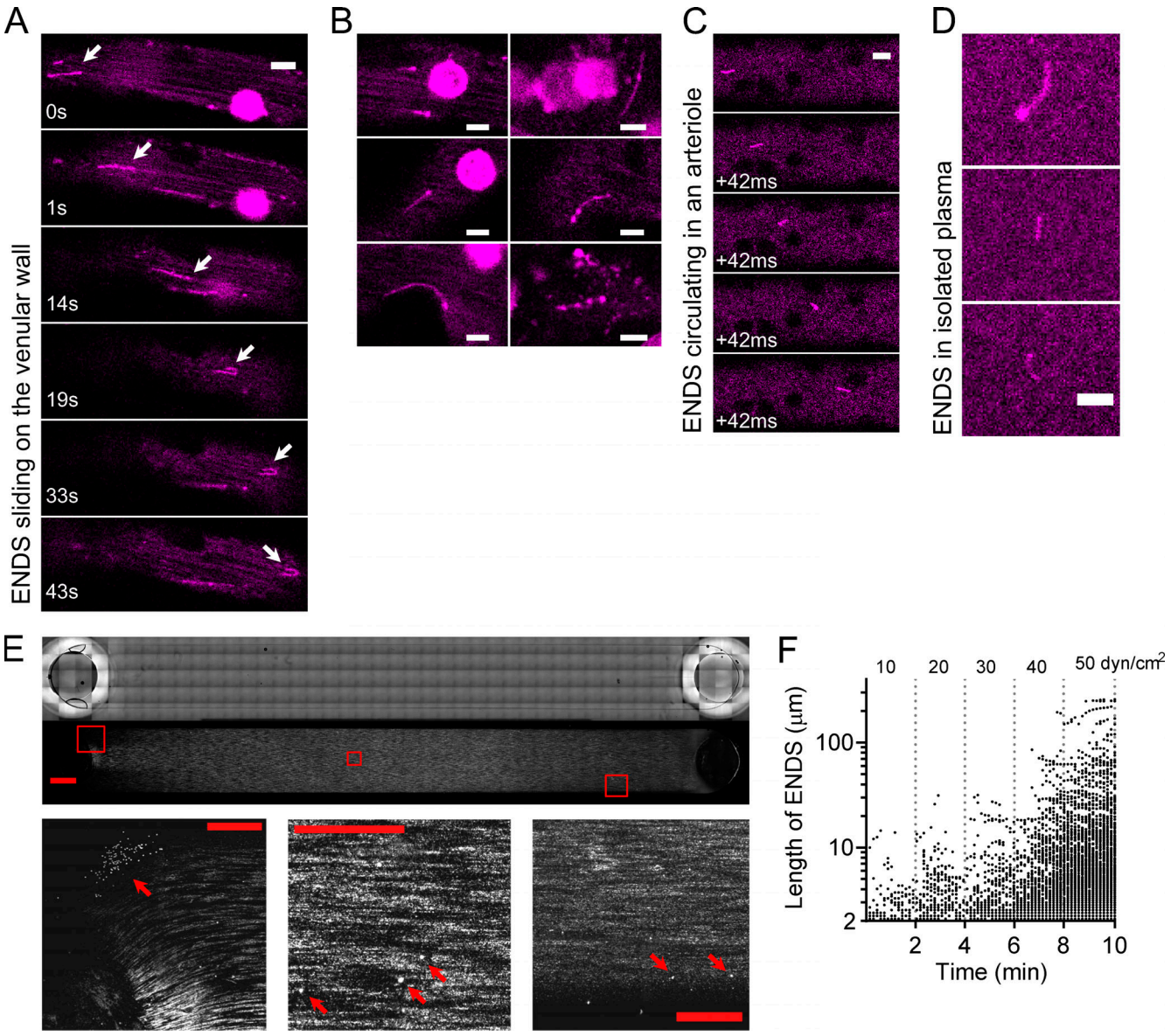

Figure S1. **Rolling neutrophils form ENDS. (A–E)** Mouse neutrophils were labeled with Ly6G-AF647. Blood flow was from left to right. **(A)** Consecutive frames show ENDS (arrows) sliding along the venular wall and then detaching. Scale bar, 8 µm. **(B)** Examples of mouse ENDS with bead-like structures in vivo. Scale bars, 6 µm. **(C)** Consecutive frames show ENDS flowing in arteriolar blood stream. Scale bar, 8 µm. **(D)** ENDS detected with confocal microscopy in isolated blood plasma. Blood was collected at the end of the imaging session via a femoral artery cannula. Scale bar, 8 µm. **(E)** After rolling of unlabeled neutrophils, the flow chamber was stained with CD16-AF647 antibody and was scanned with bright-field and fluorescent imaging. The upper panel shows the record of the entire chamber; on the upper bright-field panel, the rectangles are imaging artifact; the lower panel shows the CD16-AF647 signal to the left behind ENDS. Rectangles indicate the magnified areas. Scale bars represent 1 mm (top image) and 0.5 mm (bottom images). The spherical objects within the magnified areas (indicated by arrows) are neutrophils that remained in the flow chamber after washing. **(F)** Length of human ENDS formed during rolling on E-selectin under a WSS ramp.

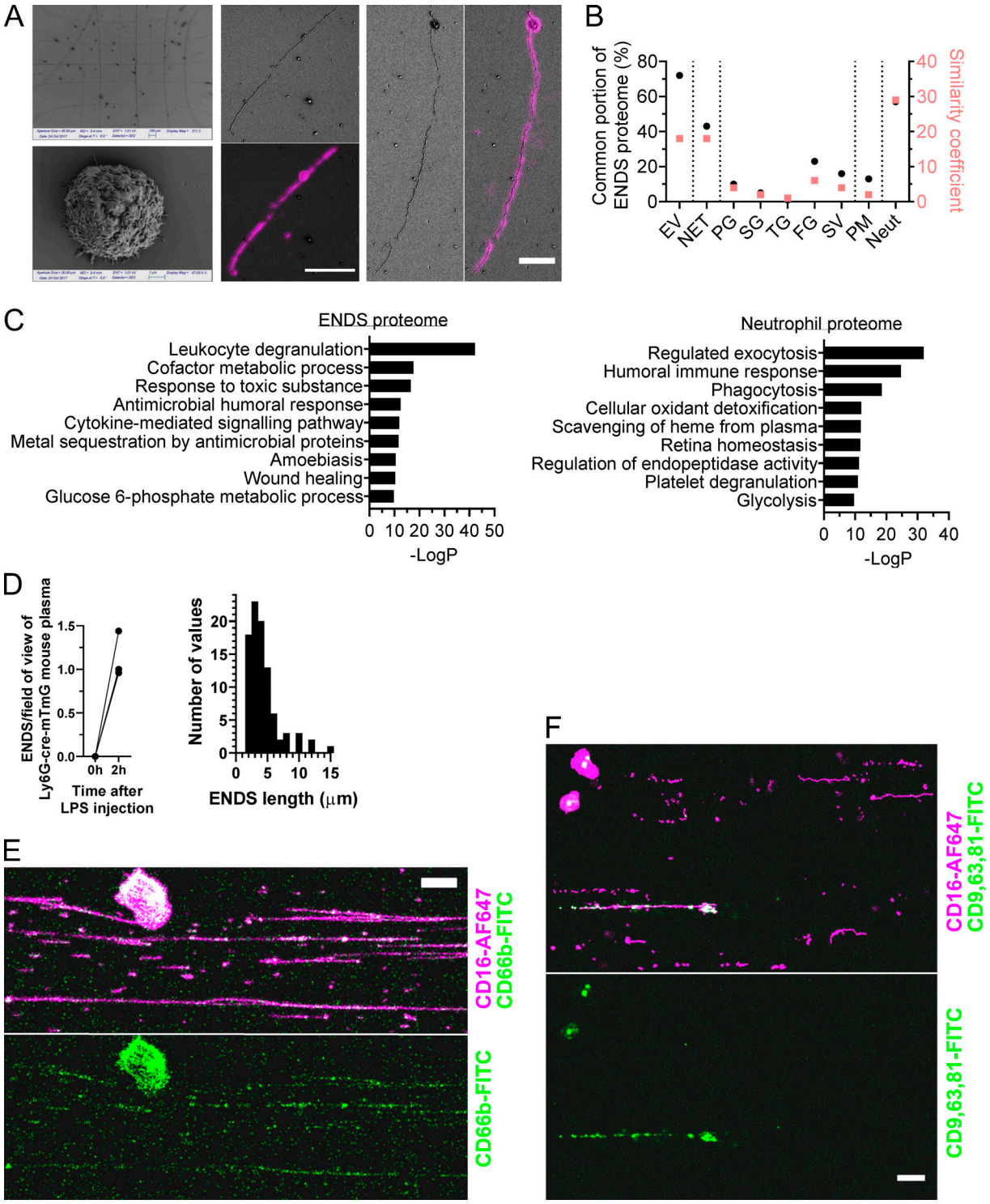

Figure S2. **Ultrastructure and composition of ENDS. (A)** SEM of a manually graded coverslip, CD16-AF647 antibody–labeled human neutrophil, or human ENDS that were centrifuged on the coverslip. Imaged with confocal microscopy and then with SEM. Left scale bar indicates 5 µm, and right scale bar indicates 3 µm. **(B)** Comparison of ENDS proteome to published proteomes of neutrophil-derived EVs, NETs, neutrophil-derived primary granules (PG), secondary granules (SG), tertiary granules (TG), ficolin granules (FG), and secretory vesicles (SV), and neutrophil plasma membrane (PM). ENDS proteome was also compared with neutrophil lysate (Neut) that was prepared from one of the donor samples that was used to makes ENDS. **(C)** Gene ontology analysis of ENDS and polymorphonuclear neutrophils proteome. **(D)** ENDS quantified with confocal microscopy in blood plasma of Ly6G-cre-mTmG mice before and 2 h after i.p. LPS injection. **(E)** Human ENDS were surface labeled with CD16-AF647 and CD66b-FITC antibodies. Top panel shows overlay of CD16-AF647 (magenta) and CD66b-FITC (green), and bottom panel shows CD66b-FITC alone. CD66b antibody-labeled ENDS, but to a weaker extent compared with CD16 antibody. Scale bar, 10 µm. **(F)** Human ENDS were surface labeled with CD16-AF647 and antibodies against TS (CD9-PE, CD63-PE, and CD81-PE). Top panel shows overlay of CD16-AF647 (magenta) and labeling for TSs (green). Bottom panel shows TS labeling alone. TSs were present only on some ENDS and in a patchy way. One example of two independent experiments are shown. Scale bar, 10 µm.

Video 1. **ENDS formation in vivo.** Mouse cremaster intravital microscopy record, a rolling neutrophil leaves an ENDS behind on the venular wall. Direction of blood flow is from right to left. The mouse was intrascrotally preinjected with TNFα to stimulate neutrophil interaction with the vasculature. Neutrophils were labeled via intravenous injection of Ly6G-AF647 antibody (magenta). Original speed, 3.62 frames/s, exported at 10 frames/s; playback speed 2.76 times faster than real speed.

Video 2. **Formation of multiple ENDS in the same vessel in vivo.** Mouse cremaster intravital microscopy record, four rolling neutrophils (examples 1-4) leave total nine ENDS behind on the wall of the same venule. Rectangles indicate the formed ENDS. Direction of blood flow is from right to left. The mouse was intrascrotally preinjected with TNFα to stimulate neutrophil interaction with the vasculature. Neutrophils were labeled via intravenous injection of Ly6G-AF647 antibody (magenta). Original speed, 4.76 frames/s, exported at 8 frames/s; playback speed is 1.76 times faster than real speed.

Video 3. **ENDS sliding and detaching from the venular wall in vivo.** Mouse cremaster intravital microscopy record, two ENDS (examples 1 and 2) sliding and detaching from the wall of the same venule are shown. Rectangles indicate where the ENDS are. Direction of blood flow is from right to left. The mouse was intrascrotally preinjected with TNFα to stimulate neutrophil interaction with the vasculature. Neutrophils were labeled via intravenous injection of Ly6G-AF647 antibody (magenta). Original speed, 4.76 frame/s, exported at 8 frames/s; playback speed is 1.76 times faster than real speed.

Video 4. **ENDS formation in a flow chamber.** Human neutrophils labeled with CD16-AF647 antibody rolled on E-selectin substrate under perfusion with Ca^{2+}/Mg^{2+} containing HBSS buffer. Flow direction is flow left to right. WSS was increased with 10 dyn/cm^2 increments to 50 dyn/cm^2. Image segmentation was applied to quantify ENDS formation; cyan – cell body, yellow – tethers that are still connected to the cell body, magenta – ENDS that are not connected to the cell body. Original speed, 3.75 frames/s; every fifth frame exported at 10 frames/s; playback speed is 13 times faster than real speed.

Table S1 and Table S2 are provided online as separate Excel files. Table S1 shows ENDS proteome analysis. Table S2 lists clinical data of septic patients.